Environmental Microbiology

ENVIRONMENTAL MICROBIOLOGY

RESEARCH ARTICLE

Microbial Ecology of Mixotrophic Chain Elongation: *Megasphaera* spp. as Drivers of Medium-Chain Carboxylate Production From H_2, CO_2, and Carboxylates

Grégoire B. L. Henry[1] | Julien Tremblay[2] | Benoit A. Stenuit[1] | Patrick A. Gerin[1]

[1]Laboratory of Bioengineering and Biorefining, Earth and Life Institute - Applied Microbiology, Université catholique de Louvain, Louvain-La-Neuve, Belgium | [2]Independent Investigator, Montreal, Canada

Correspondence: Grégoire B. L. Henry (gregoire.henry@uclouvain.be) | Patrick A. Gerin (patrick.gerin@uclouvain.be)

Received: 22 April 2025 | **Revised:** 7 January 2026 | **Accepted:** 11 March 2026

Keywords: *Clostridium ljungdahlii* | *Clostridium luticellarii* | cross-feeding activities | medium chain carboxylic acids | medium chain fatty acids | *Megasphaera elsdenii* | *Megasphaera hexanoica*

ABSTRACT

The production of medium-chain carboxylates (MCC) by mixed culture fermentation of complex organic feedstocks is often constrained by the availability of reducing equivalents. Therefore, mixotrophic fermentation processes, which integrate diverse carbon and reducing equivalents sources, are gaining more attention. However, the microbial communities evolving in such complex environments, where organic and inorganic substrates interact, remain insufficiently understood. To identify the key microorganisms involved in mixotrophic MCC production, two bioreactors were initially fed with brewer's spent grain as organic feedstock and supplemented daily with H_2 and CO_2 as inorganic substrates. Time-course analyses of net metabolite production rates and microbial community composition identified *Megasphaera* spp. (likely *M. elsdenii* and *M. hexanoica*) as the main chain elongators in the system. The results suggest that these *Megasphaera* species metabolize short-chain carboxylates, H_2 and CO_2, with potential cross-feeding interactions with acetogens (likely *Clostridium ljungdahlii* and *Clostridium luticellarii*). The homoacetogenic acetate produced is subsequently elongated, likely by *Megasphaera* species, using H_2 and CO_2 as electron and carbon sources for production of elongated carboxylates. This study paves the way for the development of MCC production strategies that integrate organic waste valorization with direct CO_2 utilization, using H_2 as an electron donor, a process that aligns with low-carbon-footprint technologies.

1 | Introduction

Microbial production of medium-chain carboxylates (MCC) is a versatile bioprocess based on chain elongation (CE) mechanisms, which can use both organic and inorganic electron and carbon sources. Many microbial cultivation techniques can be used to carry out this process, including axenic pure or mixed cultures of wild-type or engineered strains, as well as non-axenic community cultures based on defined media or using complex organic feedstock (COF) (Agler et al. 2012; Baleeiro

Abbreviations: ASV, amplicon sequence variant; AUTO, autotrophic (period); BSG, brewer's spent grain; ButOH, butanol; C2, acetate; C3, propionate; C4, butyrate; C5, pentanoate; C6, caproate; C7, heptanoate; C8, octanoate; C9, nonanoate; C10, decanoate; CE, chain elongation; $CE_{H2\&CO2}$, chain elongation phase based on H_2 and CO_2; CE_{Lact}, chain elongation phase based on lactate; $CE_{Lact\&EtOH}$, chain elongation phase based on lactate and ethanol; COD, chemical oxygen demand; COD_s, soluble chemical oxygen demand; COD_t, total chemical oxygen demand; EtOH, ethanol; FM, fresh matter; GLM, generalized linear model; Homo, homoacetogenic phase; iButOH, isobutanol; iC4, isobutyrate; iC5, isopentanoate; IndVal, indicator value; iPropOH, isopropanol; ISA, indicator species analysis; Lact, lactate; MCC, medium chain carboxylates; MIXO, mixotrophic (period); ML, mixed liquor; ND, not determined; NMDS, non-metric multidimensional scaling; PERMANOVA, permutational multivariate analysis of variance; PhC2, phenylacetate; PhC3, phenylpropionate; PropOH, propanol; r_i, metabolite (i) production or consumption rate; R1 and R2, bioreactor 1 and 2; RBO, reverse β-oxidation pathway; rTCA, reductive tricarboxylic acid cycle; SCC, short chain carboxylates; TS, total solid; VS, volatile solid.

et al. 2019; Cabau-Peinado et al. 2021; Tarasava et al. 2022; Vögeli et al. 2022; Kim et al. 2022, 2025; Gemeinhardt et al. 2025).

Heterotrophic microorganisms can convert the fermentable fractions of COF (e.g., carbohydrates, proteins, lipids) into elongated carboxylates, either with or without exogenous supply of reducing equivalents such as simple soluble carbohydrates, ethanol, or lactate (Grootscholten et al. 2013; Xu et al. 2018; De Groof et al. 2021; Kang et al. 2022; Wang et al. 2023). In contrast, autotrophic microorganisms can convert inorganic carbon sources (e.g., CO_2, CO) into carboxylates, using hydrogen (H_2) or electricity as electron donors (Jourdin et al. 2015; Batlle-Vilanova et al. 2017; Bengelsdorf and Dürre 2017; Liu et al. 2020; Baleeiro et al. 2021; Esquivel-Elizondo, Delgado, and Krajmalnik-Brown 2017). To produce MCC, both autotrophic and heterotrophic microorganisms require intracellular acetyl-CoA and reduced cofactors as key intermediates to feed the main chain elongation pathway, known as the reverse β-oxidation (RBO) (Vögeli et al. 2022; Bengelsdorf et al. 2018; Holtzapple et al. 2021; Spirito et al. 2014; Dellomonaco et al. 2011). Briefly, the RBO is a cyclic metabolic process that increases the carbon chain length of carboxylates by two carbon atoms per elongation cycle. The RBO pathway can be divided into three main stages: initiation/elongation, a series of reduction and dehydration reactions, and termination (Tarasava et al. 2022; Vögeli et al. 2022; Dellomonaco et al. 2011).

Ethanol and lactate serve as conventional electron donors, providing acetyl-CoA and reducing equivalents to feed the RBO pathway (Wang et al. 2023; Spirito et al. 2014; Angenent et al. 2016; Kucek et al. 2016). However, in organic waste streams, their concentration is often insufficient to yield significant amounts of MCC, particularly when using renewable feedstocks with high lignocellulosic content. For example, the MCC conversion yield obtained from brewer's spent grain (BSG) without the addition of any electron donor does not exceed 5% on a COD basis, even with BSG pretreated to enhance fermentability (Perimenis et al. 2018; Henry et al. 2023, 2024). Alternative strategies for supplying ethanol and lactate as exogenous electron donors should be explored, as these raw materials affect the cost-efficiency and sustainability of the process (Baleeiro et al. 2019).

One suggested strategy is to use H_2, CO_2 and/or CO as electron and carbon donors to substitute ethanol and lactate (Baleeiro et al. 2021; Nzeteu et al. 2018). For example, the combination of syngas fermentation and organic substrate conversion can trigger chain elongation. This approach could enable the complete conversion of lignocellulosic substrates into carboxylates by gasifying their unfermentable fraction into synthesis gas (syngas, i.e., CO, H_2 and CO_2) (Baleeiro et al. 2019; Ferreira et al. 2019). The syngas can then be converted by autotrophic microorganisms to acetate or ethanol through the Wood-Ljungdahl pathway, then feed chain elongator microorganisms that produced MCC. Although CO present in syngas can support carboxydotrophs and inhibit hydrogenotrophic methanogens (Esquivel-Elizondo, Delgado, and Krajmalnik-Brown 2017; Esquivel-Elizondo, Delgado, Rittmann, and Krajmalnik-Brown 2017), it can also inhibit other microorganisms of interest in a mixotrophic microbial consortium due to its toxic effects (Kroneck and Torres 2014; Oelgeschläger and Rother 2008). Carboxydotrophs, such as *Clostridium autoethanogenum*, *C. ljungdahlii*, and *C. carboxydivorans*, can tolerate CO, but primarily produce short-chain metabolites such as ethanol, acetate, butyrate, 2,3-butanediol or lactate (Bengelsdorf et al. 2018). Baleeiro and co-workers, among other studies on the mixotrophic chain elongation topic (Baleeiro et al. 2019, 2021, 2022), have recently shown that increasing CO partial pressure during mixotrophic fermentation, using corn silage as a complex organic feedstock, reshapes the microbial community and shifts the production of carboxylates with more than four carbon atoms towards predominantly acetate and propionate (Baleeiro et al. 2023).

Another strategy to produce MCC is to combine the fermentation of renewable organic residues with the use of spent CO_2 and sustainably produced H_2. The combined addition of H_2 and CO_2 has been shown to support MCC production during the fermentation of COF (Henry et al. 2023). This approach, which does not rely on CO, could promote higher microbial diversity, which is necessary to optimize the COF degradation. COF fermentation naturally generates biogenic CO_2, which can be consumed by acetogens in a mixotrophic environment to lead to the production of metabolites in a potential carbon-neutral or carbon-negative process (Hill and Papoutsakis 2025). The use of H_2 as an electron donor aligns with the decarbonization using "green" H_2 as chemical and energy vector produced from renewable electricity (Wu et al. 2022). Developing such a technology could integrate biowaste upcycling, carbon capture and utilization, and the use of low-carbon footprint H_2.

The production of MCC by integrating acidogenic fermentation of complex organic feedstocks with gas fermentation by mixotrophic microbial communities remains poorly understood. A major knowledge gap in mixotrophic chain elongation lies in identifying and understanding the dynamics of metabolically active functional microbial groups that couple autotrophic and heterotrophic pathways within the microbial network. The present study aims to identify the microorganisms involved in a mixotrophic fermentation and their interactions, with a particular focus on identifying the bacterial taxa involved in the H_2- and CO_2-based chain elongation phase, first observed by Henry et al. (2023). This process is further investigated in the present study under the same physicochemical conditions and bioreactor design.

2 | Material and Methods

2.1 | Substrate and Inoculum

Brewer's spent grain (BSG) was used as a renewable carbon-based feedstock in this study. It was collected fresh on the day of brewing at the Bertinchamps craft brewery in Gembloux, Belgium. BSG was immediately divided into 1 kg samples, which were placed in plastic bags and stored in a freezer at −20°C before use. BSG comes from the same batch as the one used in Henry et al. (2023) (Table 1). The inoculum consisted of a fresh activated sludge sample collected at the municipal wastewater treatment plant in Mont-Saint-Guibert, Belgium, on the day the fermentation started. Table 1 summarizes the BSG and inoculum composition.

TABLE 1 | Physicochemical properties of the substrate and inoculum (mean ± standard deviation of triplicate analyses): Total solid (TS) of the fresh matter (FM), volatile solid (VS) and chemical oxygen demand (COD) content of the main components of total solids.

	BSG	Inoculum
Total solid$_{105°C}$ (g_{TS}/g_{FM})	0.227 ± 0.001	0.0069 ± 0.0001
Volatile solid$_{550°C}$ (g_{VS}/g_{TS})	0.9585 ± 0.0003	0.471 ± 0.002
COD (g_{COD}/g_{TS})	1.55 ± 0.01	0.82 ± 0.02
Lignin ($g_{lignin}\ g^{-1}_{TS}$)	0.048 ± 0.001	ND
Hemicelluloses ($g_{hemicelluloses}\ g^{-1}_{TS}$)	0.331 ± 0.006	ND
Cellulose ($g_{cellulose}\ g^{-1}_{TS}$)	0.178 ± 0.002	ND
Proteins ($g_{proteins}\ g^{-1}_{TS}$)	0.251 ± 0.003	ND
Starch ($g_{starch}\ g^{-1}_{TS}$)	0.069 ± 0.002	ND
Soluble sugars ($g_{soluble\_sugars}\ g^{-1}_{TS}$)	0.0077 ± 0.0001	ND
Minerals ($g_{minerals}\ g^{-1}_{TS}$)	0.042 ± 0.001	ND
Other ($g_{other}\ g^{-1}_{TS}$)	0.70 ± 0.015	ND

Abbreviation: ND, not determined.

2.2 | Bioreactor Preparation and Monitoring

Fermentations were conducted in duplicate using 2 L Scott Duran GL45 glass bottles used as batch bioreactors, as described in Henry et al. (2023). At the start of the fermentation, the mixed liquor (ML) contained BSG at a concentration of 99 ± 0.2 $g_{COD}\ L^{-1}_{ML}$ in an initial total volume of 0.22 L_{ML}. This was achieved by adding fresh matter (FM) of BSG at a final concentration of 65.6 ± 0.1 g_{FM_BSG} (corresponding to 14.9 g_{TS} and 50.7 g_{H2O}), along with 20 mL of inoculum (0.5 $g_{COD}\ L^{-1}$), 11 mL of the concentrated mineral stock solutions, and 149.3 ± 0.1 mL of water to each bioreactor. The final concentrations of the nutrients supplemented in the bioreactor were as follows: 31 mM $NH_4H_2PO_4$, 2.9 mM $MgCl_2 6H_2O$, 0.8 mM $MgSO_4 7H_2O$, 1.4 mM L^{-1} $CaCl_2 2H_2O$, 2.7 mM L^{-1} KCl, 48 μM H_3BO_3, 75 μM $FeCl_2 4H_2O$, 6.2 μM $ZnSO_4$, 2.4 μM $MnCl_2$, 15 μM $CoCl_2$, 0.7 μM $CuCl_2$, 1.5 μM $NiCl_2$, 1.5 μM Na_2MoO_4, and 0.4 μM $Na_2Se_2O_3$, adapted from Chen et al. (2016). The initial pH of ML was 5.38 ± 0.02. It was adjusted to pH 6.8 before the beginning of the fermentation by adding 2 M KOH to each bioreactor. The pH was measured with a pH-meter (WTW pH-Electrode SenTix 41, WTW Multiline P4 universal meter). Each addition to the bioreactor was weighed with a weighing scale (OHAUS navigator NVT6201) and recorded. Before sealing the bioreactor, 10 mL of homogenized ML sample was taken with a 50 mL polypropylene syringe (BD Plastipack, USA) and stored at −80°C for further analysis. Bioreactors were then sealed and flushed for 5 min at a 4 L min^{-1} flow rate with a H_2 and CO_2 gas mixture of 77.13/22.87%$_{mol}$ (certified Crystal Mixture, Air Liquide). In each bioreactor, 20 mL of gas was sampled to identify the starting headspace gas composition and ensure that no O_2 traces remained. The gas pressure was measured with a hand manometer (UNIK 5000 manometer, GE, USA) and adjusted to 1.3 bar (absolute pressure). Bioreactors were incubated for 63 days in a thermostatically controlled incubation chamber at 35°C, in the dark, on an orbital shaker (Kühner Shaker Lab-Shaker) set to 120 rpm with a 2.5 cm amplitude.

The bioreactor monitoring routine on each day of measurements was carried out as detailed in Henry et al. (2023). Briefly, in the thermostatically controlled incubation chamber, the initial bioreactor mass and initial pressure were measured, an initial gas sample was analysed, and a 10 mL sample of the homogenized ML was collected for further analysis. Two mL of this ML sample were used to measure the pH and to determine the amount of H_3PO_4 or KOH needed to adjust the pH to 6.8. Another 2-mL sample of the ML was directly collected in 5 mL Eppendorf tubes and stored at −80°C for subsequent microbial community analyses. The remaining 6-mL sample was centrifuged, the pellet was separated and stored at −20°C, while the supernatant was directly used for soluble COD and soluble metabolites quantification; the remaining liquid fraction was then stored at −20°C. The required volume of neutralizing solution (2 M KOH or 1 M H_3PO_4) was added to the bioreactor. Distilled water was added to counterbalance the sampled volume to maintain a constant ML volume of 0.22 L throughout the fermentation. Finally, each bioreactor was flushed with the H_2 and CO_2 gas mixture and pressurized to 1.3 bar (absolute pressure).

2.3 | Chemical Analyses

Total solids, volatile solids, ash content and total COD (COD_t) were measured according to the standard methods (Standard Methods Committee of the American Public Health Association, American Water Works Association, and Water Environment Federation 2023). Soluble COD (COD_s) was measured using the COD Cell Test method (Spectroquant kits 1.14555.0001 (500–10,000 mg/L range), Spectroquant Pharo 300, Merck KGaA, Germany). The headspace gas composition was analysed by gas chromatography (CompactGC3.0, Global Analyser Solution) with a thermal conductivity detector. This gas analyser was calibrated to quantify the proportions of H_2, N_2, O_2, CO_2, CH_4 and water vapour (H_2O_v) present in the gas sample. Soluble metabolites were extracted from supernatant of the ML with liquid–liquid extraction in diethyl ether and analysed by gas chromatography with a flame ionization detector (Trace GC-FID, Thermo Scientific). The detected and quantified soluble metabolites were ethanol (EtOH), propanol (PropOH), isopropanol (iPropOH), butanol (ButOH), isobutanol (iButOH), acetate (C2), propionate (C3), butyrate (C4), isobutyrate (iC4), pentanoate (C5), isopentanoate (iC5), hexanoate (C6, also called caproate), heptanoate (C7), octanoate (C8, also called caprylate), nonanoate (C9), decanoate (C10), phenylacetate (PhC2), and phenylpropionate (PhC3). All the methods used are detailed in Henry et al. (2023). Lactic acid was quantified by high-performance liquid chromatography equipped with an Aminex HPX-87H column (300 × 7.8 mm, Bio-Rad, Hercules, USA) and a refractive index detector (Agilent Technologies 1260 Infinity, G1362A 1260 RID).

The eluent was a 5 mM H_2SO_4 solution, with a flow rate of 0.5 mL min^{-1} for 55 min. The column oven temperature was maintained at 65°C, and the RID temperature was set at 50°C. Metabolite production was normalized to the ML volume and expressed in g_{COD} $l^{-1}{}_{ML}$ (kg_{COD} $m^{-3}{}_{ML}$) to facilitate data comparison and transposition.

2.4 | Microbial Community Analysis by 16S rRNA Gene Illumina Sequencing

Microbial identification, analysis of raw absolute counts (Tremblay et al. 2015; Tremblay 2019; Tremblay and Yergeau 2019), and evaluation of functional roles in the present fermentation were performed using classical and validated methodologies. Full methodological details, including data treatment and statistical analyses, are described and referenced in the Supporting Information. The Supporting Information tables present the results of all PERMANOVA analyses using Bray-Curtis dissimilarities and relative abundances of ASVs (Tables S1–S4) and using Aitchison distances and clr-transformed absolute abundance counts of ASVs (Tables S5–S8).

3 | Results

The two bioreactors (R1 and R2) were selected out of a set of eight bioreactors operated under identical physicochemical and monitoring conditions. All eight showed a similar overall trend in MCC production, H_2 and CO_2 consumption (Figure S1). R1 and R2 were chosen as representative cases because they exhibited identical metabolite production phases but differed in production yield and temporality, allowing us to explore variability within a supposed consistent physicochemical and microbial environment. At the start of the fermentation, all bioreactors were fed with BSG as an organic substrate, inoculated with fresh activated sludge, and sparged with a mixture of H_2 and CO_2 as exogenous inorganic substrates. H_2 and CO_2 were supplied daily by adjusting the absolute pressure to 1.3 bar. The pH was adjusted to 6.8 three times a week.

The dynamics of mixotrophic microbial communities and the time course of metabolite production during BSG fermentation were monitored in depth for these two biologically replicated bioreactors (R1 and R2). Physicochemical parameters, such as pH, neutralized protons, total and partial pressure, and metabolite concentrations (in g_{COD} L^{-1} and mol L^{-1}), were monitored throughout fermentation and are presented in Figure S2. Electron and carbon balances during the autotrophic period are shown in Figure S3, while mass and COD balances across the entire fermentation process are presented in Figure S4.

3.1 | Main Metabolic Production Phases Based on Production and Consumption Rates

Figure 1 presents the metabolite production and consumption kinetics for both bioreactors. Two fermentation periods are identified based on the substrate conversion of fermentable components of BSG (starch, soluble sugars, proteins, and a fraction of lignocellulose) and the consumption of CO_2 and H_2. The first period, from day 0 to day 14, is defined as mixotrophic due to the distinct nutritional strategies in terms of utilization of carbon sources and electron donors ("Mixo" in orange in Figure 1). BSG was added only at the start of the fermentation as the organic substrate and was almost completely exhausted after 14 days of fermentation by chemoheterotrophic microorganisms, as demonstrated by Henry et al. (2023). During this period, net consumption of H_2 appeared in both bioreactors, suggesting chemolithotrophic activities (Schwartz et al. 2013). Bioreactor 1 specifically showed a clear consumption of H_2 and CO_2 concomitant with acetate production (Figure 1), indicating the simultaneous activity of homoacetogenic bacteria, which confirms the mixotrophic activities during the first period.

The second period, from day 14 to day 63 ("Auto" in blue in Figure 1) is also mixotrophic but with autotrophic dominance. Indeed, no additional BSG was introduced in the system and besides the residual BSG solid fraction that can be converted by heterotrophic microorganisms or the turnover of the microbial biomass, the major feed is the daily supply of H_2 and CO_2. During this period, the supplied H_2 and CO_2 were continuously consumed. According to the electron and carbon balance (Figure S3), the metabolites produced during the autotrophic period correspond to at least 82%–85% of the supplied H_2 and 83%–86% of the supplied CO_2, confirming that the metabolism during this second phase was predominantly autotrophic.

Based on the uptake and secretion rates of substrates and metabolites in the fermentation broth, five metabolic phases were identified (Figure 1): hydrolysis and acidogenesis, chain elongation based on lactate and/or ethanol ($CE_{Lact\&EtOH}$ in brown), chain elongation based on H_2 and CO_2 ($CE_{H2\&CO2}$ in pink), homoacetogenesis (Homo in grey), and methanogenesis. Methanogenic phases are not indicated on Figure 1 due to the low methane production observed, which started after day 51 for bioreactor 1 and day 42 for bioreactor 2. Hydrolysis and acidogenesis are not depicted in Figure 1 as they are preliminary processes mainly occurring during the mixotrophic period converting BSG into primary metabolites (lactate, ethanol, and SCC).

During the mixotrophic period, the first phases of chain elongation occurred when lactate was consumed between day 2 and 4 in bioreactor 1, and when lactate and ethanol were successively consumed between day 2 and 9 in bioreactor 2 (Figure 1, $CE_{Lact\&EtOH}$ brown area). In bioreactor 1, a homoacetogenic activity was observed during the mixotrophic period between day 4 and 7, characterized by the consumption of H_2 and CO_2 and the production of acetate (Figure 1). Acetate was then immediately consumed, along with H_2 and CO_2, to produce butyrate, valerate, and caproate until day 11. This pattern is characteristic of a chain elongation phase based on SCC, H_2, and CO_2 as previously described by Henry et al. (2023). In contrast, bioreactor 2 entered a stationary phase from days 9 to 14 after the observed lactate and ethanol-based CE phase, with no net metabolite production or consumption.

The autotrophic period began for both bioreactors after the organic substrate (BSG) was mostly exhausted, with a homoacetogenic phase characterized by a clear consumption of H_2 and CO_2 concomitant with the production of acetate (Figure 1). After this

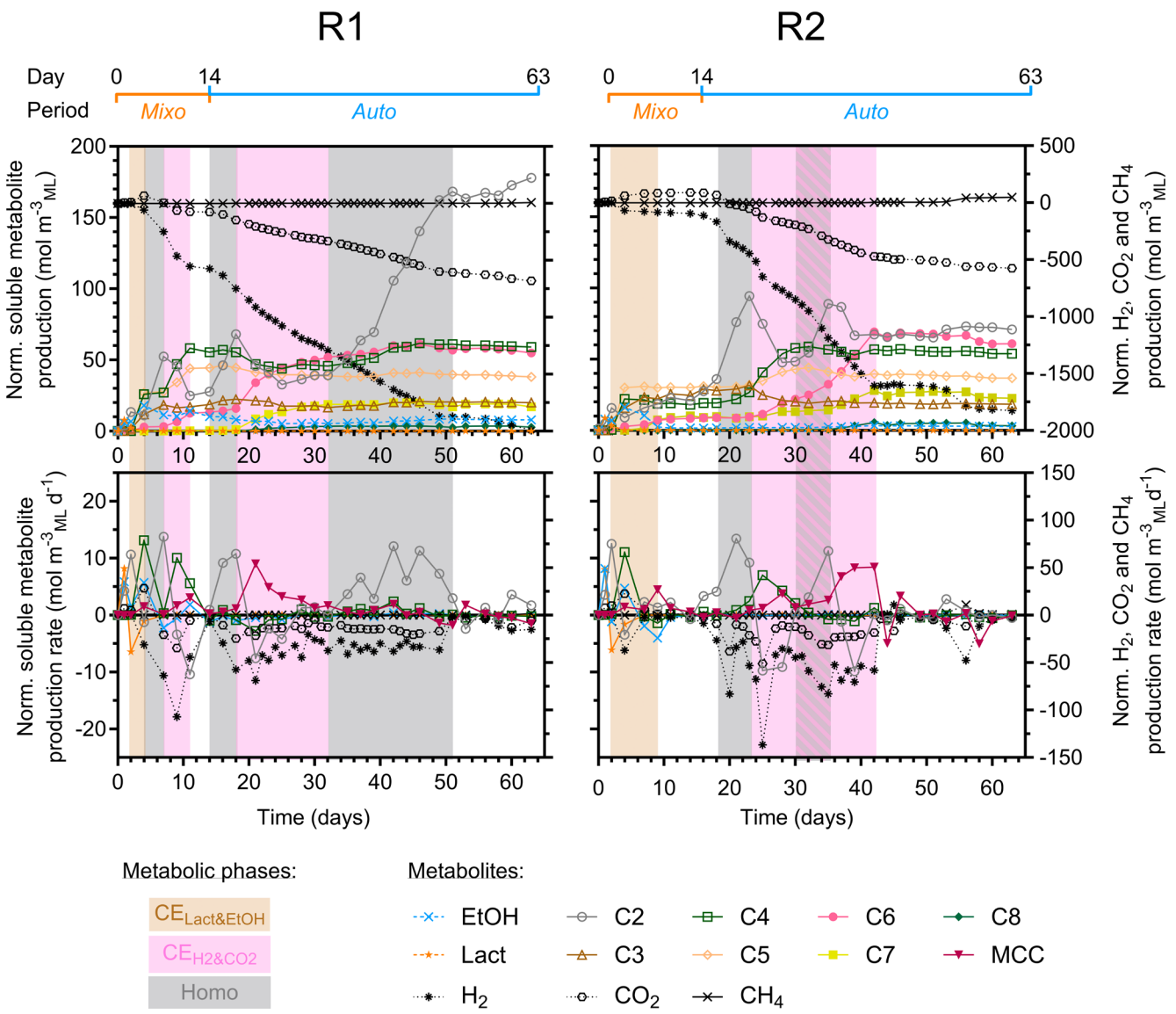

FIGURE 1 | Cumulative metabolite production (in mol; top) and time-interval average productivity (in mol d^{-1}; bottom), both normalized to the mixed liquor volume (in m^3_{ML}), over the 63-day fermentation period for bioreactor 1 (R1, left) and bioreactor 2 (R2, right). Negative productivity values indicate net consumption. The results are divided into two periods based on the organic substrate, H_2 and CO_2 consumption (mixotrophic period from day 0 to day 14 (*Mixo*—orange), and the autotrophic period from day 14 to 63 (*Auto*—blue)). Main metabolic phases are identified based on metabolite production or uptake rates and are highlighted by coloured areas: chain elongation based on lactate or/and ethanol ($CE_{Lact\&EtOH}$, brown), chain elongation driven by H_2 and CO_2 ($CE_{H2\&CO2}$, pink), and homoacetogenesis (*Homo*, grey). Metabolites are abbreviated as follows: Lact (lactate); EtOH (ethanol); C2 (acetate); C3 (propionate); C4 (butyrate); C5 (valerate); C6 (caproate); C7 (heptanoate); C8 (octanoate).

homoacetogenic phase, the production of metabolites differed between the two bioreactors.

In bioreactor 1, from day 18 to day 32, the main products were medium-chain carboxylates (MCC; C6–C8), which were produced through the consumption of short-chain carboxylates (SCC; C2–C5), H_2 and CO_2 (Figure 1—R1). Day 32 marked a significant shift in the production phase, transitioning from mainly producing MCC to primarily producing acetate. Homoacetogenesis remained active until days 49–51, when methanogenesis began to emerge slightly.

Bioreactor 2 primarily produced butyrate and valerate, from day 23 to day 30, along with a small amount of MCC, by consuming acetate, propionate, H_2, and CO_2. Distinct acetate production was observed from day 30 to 35, during the chain elongation period driven by H_2 and CO_2. Acetate was then consumed along with propionate, butyrate, valerate, H_2, and CO_2 to produce mainly MCC (C6–C8) until day 42. This coincides with the onset of methanogenesis.

After day 51 for bioreactor 1 and day 42 for bioreactor 2, carboxylate production stopped, and the remaining gas consumption was mainly linked to the methane production (Figure 1). To avoid electron misrouting towards CH_4 production, the pH was lowered to 5.5 by adding H_3PO_4 aiming at inhibiting methanogens. In both bioreactors, acidification only temporarily stopped methanogenesis. Both bioreactors were stopped on day 63 because of the reduced fermentation and chain elongation activities.

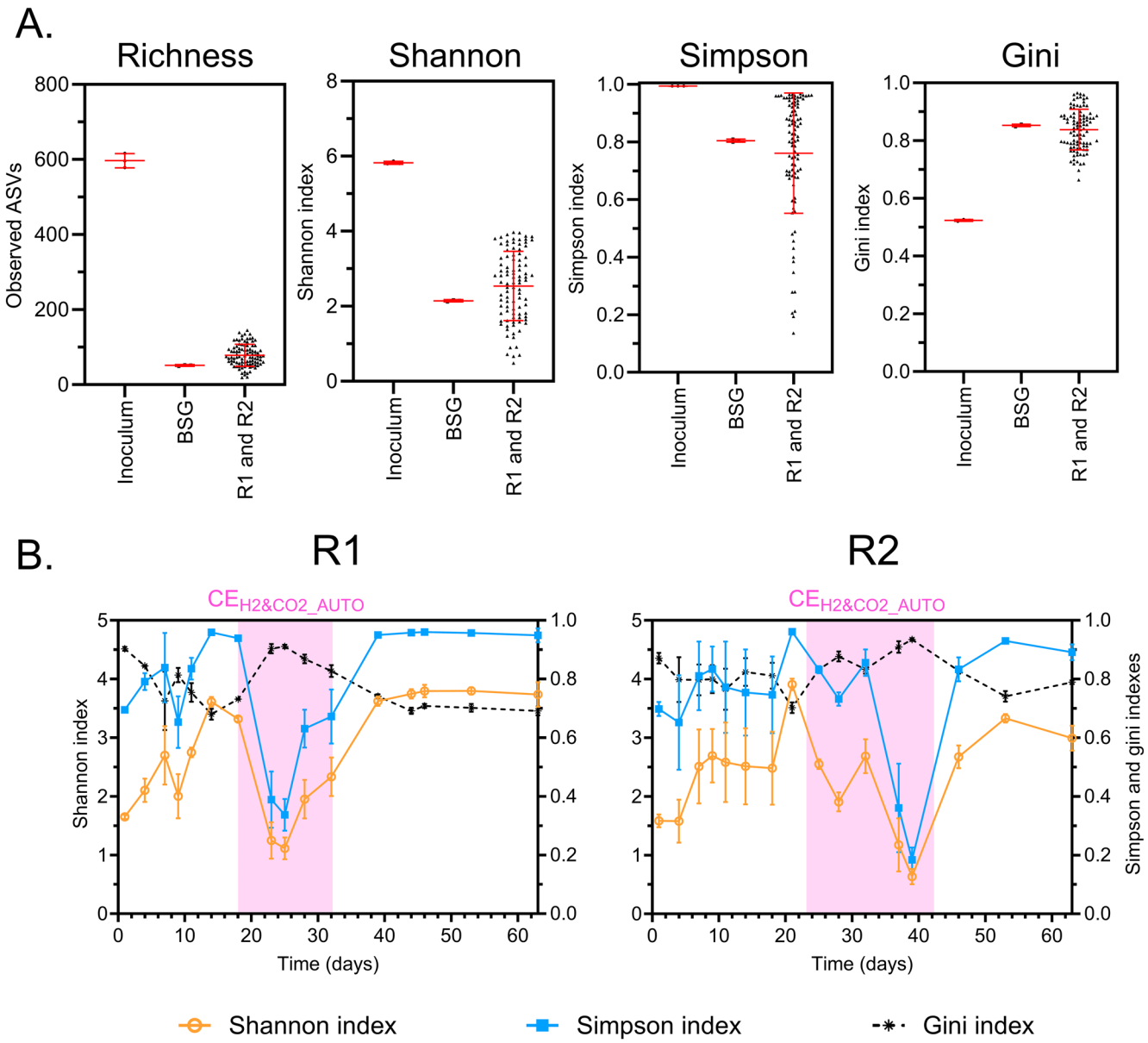

FIGURE 2 | Microbial community diversity metrics calculated from a rarefied ASV table normalized to a sequencing depth of 2000 reads. (A) Richness (observed ASVs), Shannon index, Simpson's dominance index, and Gini coefficient for the initial inoculum, the native microbiome of BSG samples, and both bioreactors (R1 and R2). (B) Temporal evolution of the Shannon (orange solid line, open circles), Simpson (blue solid line, filled squares) and Gini coefficients (black dotted line, crosses) during fermentation in bioreactor 1 (R1, left) and 2 (R2, right). The pink shading indicates the H_2&CO_2-based chain elongation phase identified during the autotrophic period ($CE_{H2\&CO2\_Auto}$), as described in Section 3.1.

In conclusion, MCC accumulated to maximum concentrations of 15.8 and 19.2 g_{COD} $L^{-1}{}_{ML}$ in the fermentation broth of bioreactor 1 (at day 32) and bioreactor 2 (at day 42), respectively (Figure S2). This corresponds to 39.7 $mmol_{C6}$ $l^{-1}{}_{ML}$, 15.0 $mmol_{C7}$ $l^{-1}{}_{ML}$ and 2.9 $mmol_{C8}$ $l^{-1}{}_{ML}$ for R1 and 47.6 $mmol_{C6}$ $l^{-1}{}_{ML}$, 18.2 $mmol_{C7}$ $l^{-1}{}_{ML}$ and 4.1 $mmol_{C8}$ $l^{-1}{}_{ML}$ for R2. On day 63, the cumulative net MCC production reached 75.1 and 86.9 mol (normalized to the mixed liquor volume (in $m^3{}_{ML}$)) in bioreactors 1 and 2, respectively. For both bioreactors, caproate (C6) was the predominant MCC, with a normalized cumulated net production of 54.9 and 60.8 mol_{C6} $m^{-3}{}_{ML}$ in bioreactors 1 and 2, respectively. In addition, the maximum average time-interval normalized MMC productivity reached 9.03 mol $m^{-3}{}_{ML}$ d^{-1} in bioreactor 1 (between days 18 and 21) and 8.4 mol $m^{-3}{}_{ML}$ d^{-1} in bioreactor 2 (between days 39 and 42).

3.2 | Dynamics of Microbial Community Composition and Detection of Significant Taxa Across Metabolic Phases and Sample Types

3.2.1 | Microbial Community Composition at Genera Level

Fermentation began with coalescence of endogenous BSG microbial community and fresh activated sludge in the two batch reactors. The initial inoculum exhibited greater microbial diversity than endogenous BSG, with 597 ± 19 observed ASVs for the inoculum and 51 ± 2 observed ASVs for BSG (Figure 2A). The initial inoculum and BSG samples had Shannon indices of 5.82 ± 0.04 and 2.15 ± 0.03, respectively (Figure 2A). Microbial compositions of the fresh activated sludge (inoculum) and BSG

are shown in Figures S5 and S6. *Archaea* were detected in the inoculum at a relative abundance of 0.11% ± 0.03%. In the BSG samples, the *Bacillaceae* family was detected at a high relative abundance (92% ± 1%), mainly represented by *Bacillus* sp.; 41% ± 1%. These spore-forming *Bacillus* sp. are known to grow on BSG (Kotlar et al. 2011; Łaba et al. 2017) and are part of the endogenous BSG microbial community (Bianco et al. 2024; Carvalheira et al. 2022). Common beer-spoilage bacteria (Paradh et al. 2011; Juvonen 2015; Suzuki 2015) were identified at low levels, including members of the *Lactobacillaceae* family (e.g., *Lactobacillus* sp. with a relative abundance of 3.9% ± 0.3%) and the *Veillonellaceae* family (e.g., *Megasphaera* sp. with a relative abundance of 0.05% ± 0.01%). Based on the Gini coefficient (Figure 2A), the microbiome of BSG samples (Gini = 0.902 ± 0.007) shows lower evenness than the inoculum (0.617 ± 0.012). This confirms that the brewing process exerts selective pressure during BSG production. This result also supports the expected high biodiversity of activated sludge.

For both bioreactors, richness based on observed ASVs ranges from 19 to 145, while the Shannon and Simpson indices fluctuate from 0.48 to 3.97 and from 0.13 to 0.96, respectively (Figure 2A). These changes throughout the fermentation suggest a succession of different nutritional and metabolic phases catalysed by specific functional groups of phylogenetically distinct microorganisms. Both the Simpson's dominance index and the Shannon index demonstrated a marked decline in biodiversity during the autotrophic H_2 and CO_2 chain elongation phase, indicating the dominance of specific taxa, as confirmed by the high Gini coefficient values (Figure 2B). During BSG fermentation under selective anaerobic conditions with a pressurized headspace, the microbial communities remain uneven compared to the inoculum, showing the greatest unevenness during the elongation phase with H_2 and CO_2 (Figure 2B).

A total of 71 genera were identified with a relative abundance greater than or equal to 1% in at least one of the samples analysed for microbiome characterization. In bioreactor samples, 46 genera met this criterion. The evolution of the relative abundances of the 25 most abundant taxa at the genus level for bioreactors 1 and 2 is presented in Figures S7 and S8. Among these, 17 genera, shared between both bioreactors, belong to *Firmicutes*, *Bacteroidota* and *Actinobacteriota*, collectively accounting for 61% ± 27% across all bioreactor samples. *Megasphaera* was the most abundant genus throughout the entire fermentation period, with a relative abundance of 30% ± 33%, peaking during the chain elongation phases despite significant variability.

During the mixotrophic period, both bioreactors were dominated by bacterial genera linked to lactate production and consumption, such as *Lactobacillus* (Pot et al. 2014), *Streptococcus* (du Toit et al. 2014), *Bifidobacterium* (Egan 2018), *Weissella* (Fusco et al. 2015), *Olsenella* (Dewhirst et al. 2001) *and Dialister* (Wade 2015), and heterotrophic carbohydrate-degrading bacteria, including *Prevotella and Prevotella* 7, recently reclassified into the genera *Segatella*, *Hallella*, and *Leyella* (Hitch et al. 2022; Shah et al. 2015) (Figures S7 and S8). The *Megasphaera* genus reached a high relative abundance on day 4, when lactate was consumed (Figure 1), at 31% ± 15% in bioreactor samples (Figures S7 and S8). In bioreactor 1, on days 9 and 11, during the mixotrophic H_2- and CO_2-based CE phase, *Megasphaera* accounted for 60% ± 18% of the microbial community.

During the H_2- and CO_2-based chain elongation phase of the autotrophic period, *Megasphaera* was the most abundant genus, with a relative abundance of 77% ± 11% and 79% ± 13% in bioreactors 1 and 2, respectively. *Clostridium sensu stricto 12* and *Caproiciproducens* were present during the homoacetogenic phases (day 14–18 and 32–51 for bioreactor 1; day 18–23 and 30–35 for bioreactor 2). During homoacetogenic phases, *Clostridium sensu stricto 12* had a mean relative abundance of 7.8% ± 4.1% and 2.4% ± 1.1%, and *Caproiciproducens* reached 9.4% ± 5.7% and 1.7% ± 0.8% in bioreactors 1 and 2, respectively (Figures S7 and S8).

Beta diversity analysis using NMDS and Bray–Curtis similarity indices (Figure 3) revealed clear clustering of samples according to the main metabolic phases. Three primary subgroups were distinguished: the inoculum, the endogenous BSG microbiome, and acidogenesis samples (at day 1), with the latter separated from both the inoculum and BSG microbiome, reflecting a rapid shift in microbial composition due to microbial community coalescence and the imposed selective pressure (Liu and Salles 2024). On day 4, the ethanol- and lactate-based CE subgroup is also separated, confirming rapid community compositional changes under environmental selection. From day 4 to day 14, samples from the mixotrophic period (crosses) clustered tightly in the top-right section of the graph, including the ethanol- and lactate-based CE subgroup, the mixotrophic H_2- and CO_2-based CE (Elong_H2CO2_Mixo) subgroup and the homoacetogenesis_Mixo subgroup. This indicates convergence and compositional similarity of the microbial community. In contrast, autotrophic samples (open triangles) from day 14 to day 63 formed a more dispersed cluster below, with distinct separation of autotrophic H_2 and CO_2-based CE (Elong_H2CO2_Auto) and methanogenesis subgroups, showing significant compositional variations. Interestingly, homoacetogenesis subgroups (grey fill, Figure 3) overlapped across ethanol- and lactate-based CE, H_2- and CO_2-based CE and methanogenesis subgroups, suggesting simultaneous homoacetogenic activity (Figure 3). The proximity of the centroids of the ellipses encompassing all samples from each bioreactor, R1 and R2, further indicates similarities between the microbial communities in the two bioreactors. A similar figure specifying the bioreactor origin of each sample is provided in Figure S9.

PERMANOVA (adonis2, 999 permutations, Bray-Curtis distances) using the grouping variables shown in Figure 3 (BSG, inoculum, and metabolic phases) on the dataset used for the NMDS ordination revealed significant differences in microbiome composition between groups. Grouping factors explained 62.6% of the variation in community composition (Figure 3). Excluding the BSG and inoculum samples in the grouping factors, similar results were obtained ($R^2 = 0.572$, $F = 17.8$, $Pr(>F) = 0.001$). Pairwise PERMANOVA post hoc tests indicated that metabolic phases differed significantly from each other (adjusted $p < 0.02$), except for the comparison between ethanol- and lactate-based chain elongation and homoacetogenesis_Mixo, highlighting the compositional shifts observed in the NMDS analysis (Figure 3). Comparable patterns were observed when using clr-transformed abundance tables with Aitchison

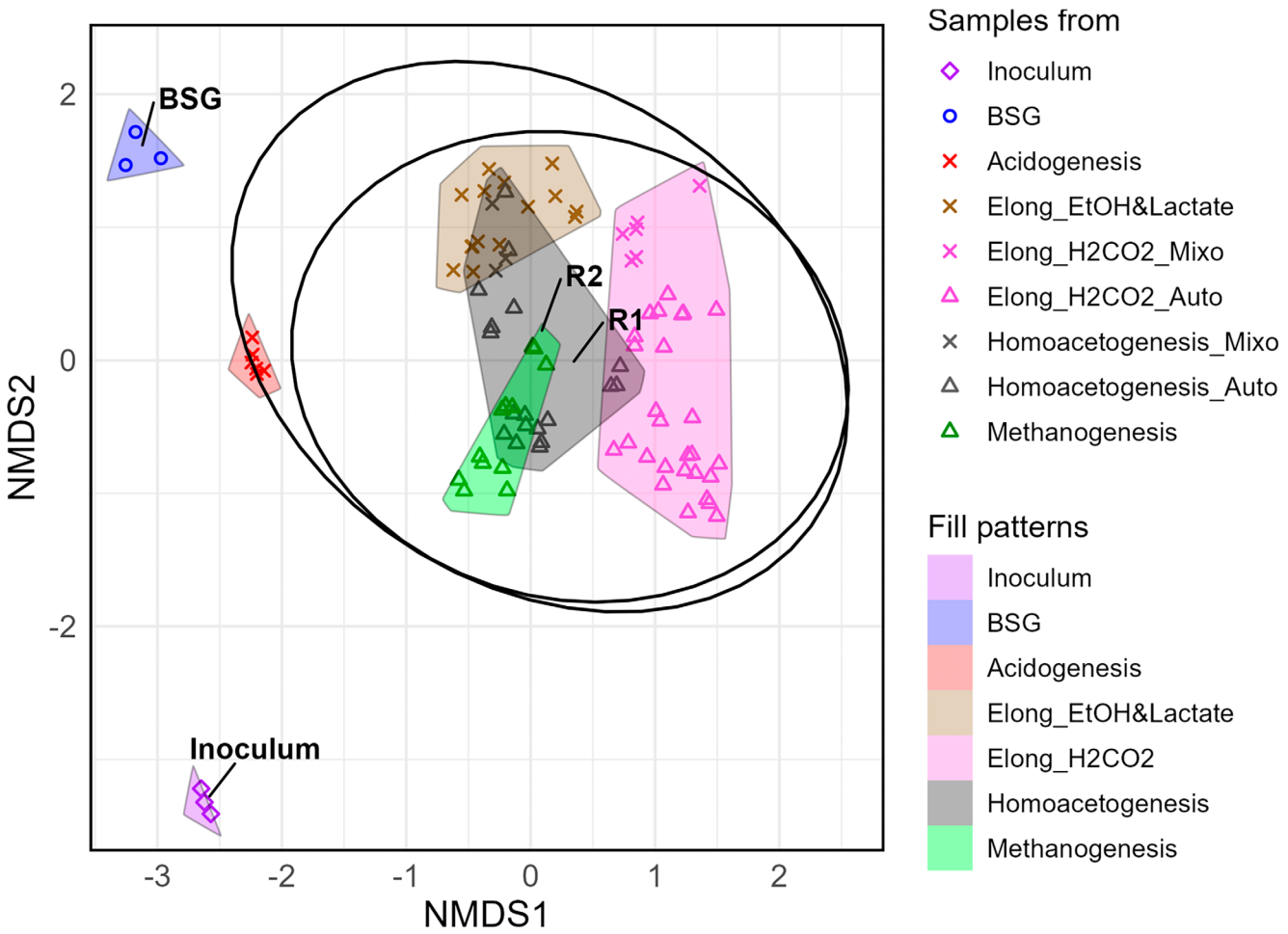

FIGURE 3 | Non-metric Multidimensional Scaling (NMDS) of microbiome profiles for each technical sample from bioreactors 1 and 2, the inoculum and BSG samples. Marker shapes indicate sample types: inoculum (open diamonds), initial BSG sample (open circles), mixotrophic period (crosses) and autotrophic period (open triangles). Marker colours and fill patterns represent the metabolic phase or sample origin: inoculum (purple), initial BSG sample (blue), acidogenesis (red), lactate- and/or ethanol-based chain elongation (brown), H_2- and CO_2-based chain elongation (pink), homoacetogenesis (grey), and methanogenesis (green). Black ellipses show the 95% confidence region for each reactor, and the labels Inoculum, BSG, R1 and R2 mark the centroids (mean NMDS coordinates) of the corresponding groups. Permanova using the grouping variables shown in this figure ("Samples from") was significant ($R^2 = 0.62597$, $F = 17.572$, $Pr(>F) = 0.001$).

(Euclidean) distances, confirming that these community differences are robust to the choice of normalization and distance metric (Figure S10).

3.2.2 | Significant Taxa Identification and Taxa Assignment

3.2.2.1 | Taxa Assignment With Silva and Geneious Prime BLASTn Method. All ASVs were identified at the genus level using the Silva database. Those significantly associated with a metabolic phase or period, as determined by at least one of the methods cited above and being part of the 25 most abundant ASVs at the "silva database"-genus level, were identified as the genus and species with the best match obtained through BLASTn in Geneious Prime using the 16S ribosomal rRNA gene collection. All genus and species identifications using the Silva database and the Geneious Prime BLASTn method are summarized in the "Supplementary Summary table—ASV sp." sheet of the Supporting Infortmation excel file. The evolution of their relative abundance through the entire fermentation can be followed using the "RelAb Dynamics" sheet of the Supporting Infortmation excel file.

Although the V4 region of 16S rRNA gene alone cannot guarantee species-level resolution, the two ASVs (ASV1 and ASV2) are presumed to correspond to *Megasphaera hexanoica* and *Megasphaera elsdenii* (sharing 99% and 100% identity with their assigned species). These two ASVs share only 95% identity, with 12 nucleotide differences across the 252 bp V4 region (Figure S11). This level of divergence is well below the commonly accepted thresholds for species identity (> 98.5% for 16S rRNA gene V3–V4 region (Wang et al. 2025), and ~100% for 16S rRNA gene V4 region alone (Edgar 2018)), which strongly supports that these ASVs represent distinct species. Therefore, although species-level assignment should be interpreted with caution, the genetic distance between ASV1 and ASV2 justifies their discrimination. In contrast, ASV2, ASV27, and ASV30 were all identified as *Megasphaera elsdenii* with sequence

identities of 100%, 99.8%, and 99.6%, respectively, differing by only 1–2 nucleotides, suggesting that they all likely belong to the same species (Figure S11).

Although the V4 region of the 16S rRNA gene does not provide absolute species-level resolution, species names are used with caution throughout the manuscript for readability. To ensure transparency, all ASVs and their corresponding taxonomic assignments (including identity percentages) are provided in the sheet "Summary table—ASV sp." of the Supporting Infortmation excel file.

3.2.2.2 | Bioindicator Species. Significant taxa are interpreted as key contributors (players) or potential bioindicators of shifts in microbial community composition and function, as they exhibit statistically significant differences in abundance across conditions or metabolic phases. Three methods were used to detect significant taxa: (i) ASV coefficients from a linear model (R Stats Package; Figures S12 and S13, Table S9), (ii) indicator species analysis (ISA) by Dufrêne and Legendre (1997), and (iii) generalized linear model (GLM) with negative binomial distribution in DESeq2 (Figures S14–S17).

The linear model (Table S9) shows that species within the *Megasphaera* genus, especially ASV1 and ASV2 (presumably *M. hexanoica* and *M. elsdenii*) are significant during the different CE phases. *M. hexanoica* is significant only in the autotrophic period and the autotrophic H_2- and CO_2-based CE phase, while *M. elsdenii* is significant in both nutritional periods, specifically during H_2- and CO_2-based CE phases and the ethanol- & lactate-based CE phase (Figures S12A,B and S13B–D).

The ISA confirms ASV1 (likely *M. hexanoica*) has strong association with the H_2- and CO_2-based chain elongation phase, with an indicator value of 0.93 ($p = 0.001$) using a binary grouping variable (Elong_H_2CO_2 vs. Others). ASV1 demonstrates a specificity of 94.9% and a selectivity of 90.9% with the Elong_H_2CO_2 group. Differential abundance analysis using DESeq2, based on pairwise comparisons between sample groups (Figures S14–S17), estimated $\log_2$ fold changes and identified ASV1 as the taxon most significantly associated with: (i) the autotrophic period (versus mixotrophic, Figure S14), (ii) the H_2&CO_2-based CE phases (versus mixotrophic CE phases, Figure S15) and (iii) the autotrophic H_2&CO_2-based CE phases (versus all metabolic phases occurring during the autotrophic periods Figure S16).

According to the indicator species analysis (ISA), ASV2 (likely *M. elsdenii*) was not identified as an indicator species for any specific metabolic phase or period, suggesting a transversal role throughout the entire fermentation. Moreover, DESeq2 pairwise comparisons showed ASV2 was not significantly associated neither with the mixotrophic period nor the autotrophic one. In contrast, ASV2 is significantly associated with (i) mixotrophic CE phases compared with all other mixotrophic metabolic phases, Figure S15 and (ii) the autotrophic H_2&CO_2-based CE phases compared with all other autotrophic metabolic phases, Figure S16. This supports the linear model, indicating that ASV2 (likely *M. elsdenii*) is a key player during the ethanol- and lactate-based CE and the H_2&CO_2-based CE phases (Figure S13B–D). Overall, these results support the hypothesis that both species are involved in H_2- and CO_2-based chain elongation.

The linear model shows that ASV15, ASV17 and ASV25 (presumably assigned to *Clostridium luticellarii* and *Caproiciproducens galactitolivorans*) are within the ten most significant taxa during the autotrophic homoacetogenic phases (Figure S13F), while ASV10 (likely *C. ljungdahlii*) presents the thirteenth highest coefficient in the mixotrophic homoacetogenic phase (data not shown). The ISA performed using the binary grouping variable Homoacetogenesis vs. Others yielded indval values of 0.85 and 0.86 ($p = 0.001$), respectively, for ASV10 and ASV15. These high indicator values indicate a strong association of both taxa with the homoacetogenic phase, with specificities of 84% and 87% for ASV10 and ASV15, respectively. Moreover, ASV10 and ASV15 (likely *C. ljungdahlii* and *C. luticellarii*) were significantly associated with the autotrophic period (versus mixotrophic period Figure S14). This is aligned with the linear model and the ISA outcomes and supports the hypothesis that ASV10 and ASV15 are involved in homoacetogenesis.

The results from all three methods (linear model, ISA, and DESeq2) converge to indicate that ASV1 (likely *Megasphaera hexanoica*) and ASV2 (likely *Megasphaera elsdenii*) are suggested to be key microorganisms involved in H_2- and CO_2-based CE and ethanol- & lactate-based CE, while ASV10 (likely *C. ljungdahlii*) and ASV15 (likely *C. luticellarii*) are suggested to be key microorganisms during the homoacetogenic phases. These findings will be discussed in the following section, with a focus on these four ASVs. Other microorganisms, such as *Eubacterium* (ASV33), *Caproiciproducens* (ASV17 and 25), *Bifidobacterium* spp., and *Prevotella* spp., may also play secondary roles and will be highlighted where relevant.

3.2.2.3 | The 25 Most Abundant Taxa of the Microbial Communities. Figure 4 shows the 25 most abundant ASVs detected across both bioreactors. Eighteen of these ASVs were among the top ten significant taxa identified using the linear model during specific periods and metabolic phases (Table S9). The ASVs are hierarchically clustered in a horizontal manner based on their co-occurrence across metabolic phases, and in a vertical manner based on reactor presence (Reactor), nutritional periods (Metabolism_Carbon), and metabolic phases (Main_Metabolic_Phase). This shows that there are similar community compositions within each group. Figure 5 shows the relative abundance of 12 key taxa identified throughout the specific metabolic fermentation phases: the $CE_{H2\&CO2}$, $CE_{ETOH\&Lact}$, homoacetogenesis, and methanogenesis phases.

During the mixotrophic period, for both bioreactors, ASV2 (likely *M. elsdenii*) emerged as a dominant species alongside lactic acid-producing and consuming bacteria, as well as heterotrophic carbohydrate and protein-degrading bacteria (Figure 4, Table S9). On day 4, when both bioreactors clustered closely on the dendrogram (Figure 4), ASV2 accounted for 30% ± 14% of all taxa (Figure 5).

In bioreactor 1, days 7, 9 and 11 form a cluster representing the transition from a homoacetogenic to a H_2- and CO_2-based CE phase (Figure 4). On day 7, which showed the highest acetate production rate (Figure 1: 13.8 mol m^{-3} d^{-1}), ASV10 (likely *C. ljungdahlii*) appeared at 1.6% ± 0.9% relative abundance (Figure 5). During the subsequent mixotrophic H_2- and CO_2-based CE phase (from day 9 to day 11), ASV2 (likely *M. elsdenii*)

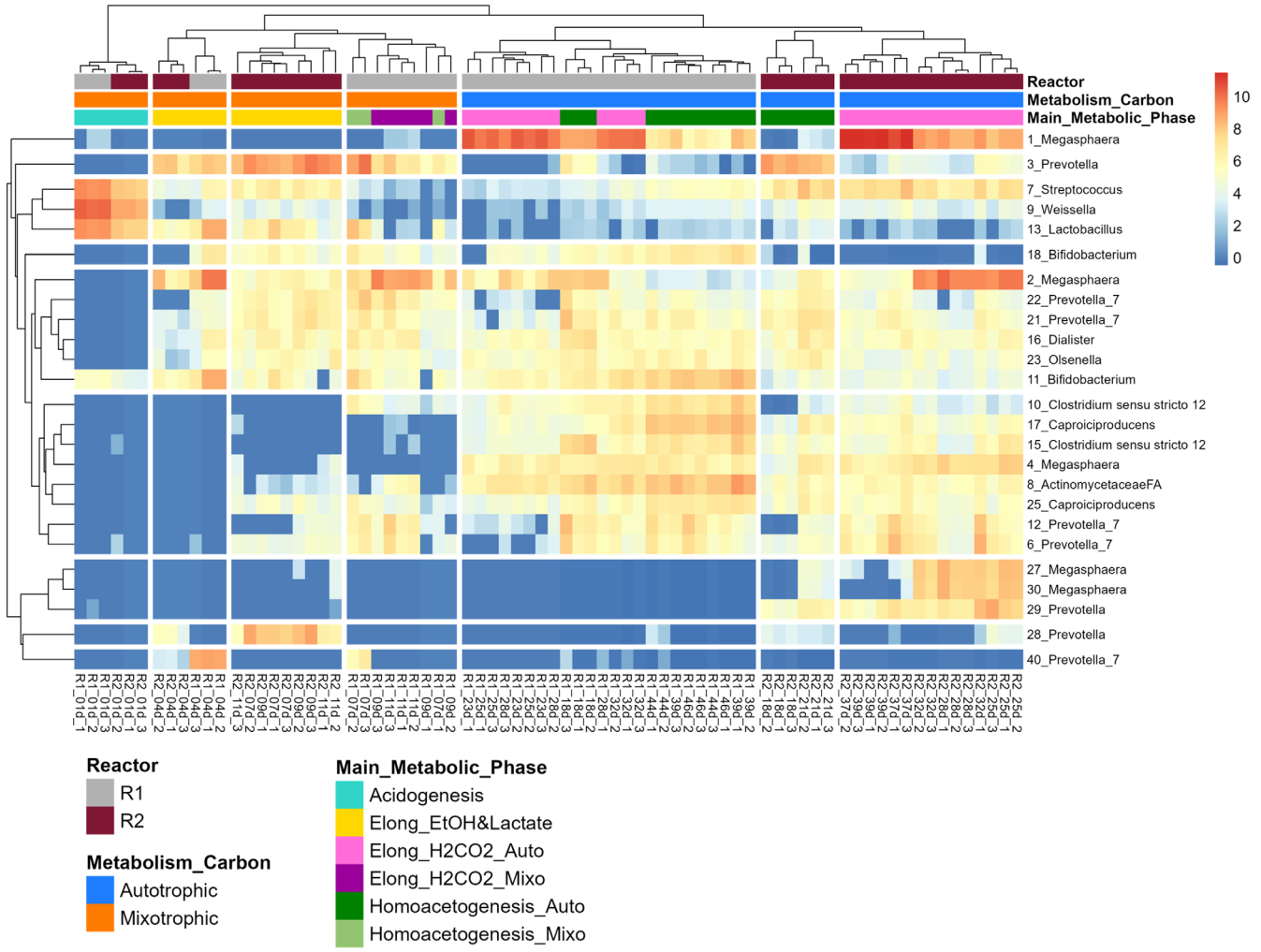

FIGURE 4 | Heatmap of the 25 most abundant ASVs present across different periods and main metabolic phases of fermentation in both bioreactors. Coloured squares represent clr-transformed abundances (log-ratios relative to the community geometric mean) of each ASV. Colour intensity reflects clr-transformed abundance, with higher values in red and lower values in blue (see colour scale legend; minimum clr of around −0.46, maximum clr of around 11.5). The x-axis clusters samples based on microbial community composition similarity, and is annotated for bioreactors, carbon metabolism type (autotrophic or mixotrophic), and main metabolic phases. ASVs on the y-axis are clustered according to their co-occurrence patterns across samples.

resurged, rising from 6.6% ± 4.0% (day 7) to 59.3% ± 7.3% (day 9) before declining to 6.4% ± 2.0% on day 14 (Figure 5).

In bioreactor 2, during the mixotrophic period, samples from days 7, 9, and 11 also clustered together (Figure 4). The heterotrophic carbohydrate-degrading bacteria identified as *Prevotella* genus (mainly ASV3 and ASV28) were among the most abundant ASVs (Figure 4, Figure S8). ASV33 (*Eubacterium* [nodatum group]) was also prevalent from day 7 to day 14, with an average relative abundance of 4.2% ± 3.5% (Figure 5, Figure S8). ASV33 is closely related to *Aminicella lysinolytica* (identity 96.6%) or *Eubacterium pyruvativorans* (identity 95.6%) based on BLASTn search in the 16S rRNA gene database.

The autotrophic period after day 14 encompasses the main metabolic phases: homoacetogenesis, H_2- and CO_2-based CE, and methanogenesis. This period was mainly dominated by the *Megasphaera* genus, including ASV1 (likely *M. hexanoica*), ASV2, ASV27, and ASV30 (likely *M. elsdenii*) as well as ASV4 (likely *M. sueciensis*). *Clostridium sensu stricto 12* genus was represented by ASV10 (likely *C. ljungdahlii*), ASV15, and ASV54 (presumably associated with *C. luticellarii*), along with ASV17 and ASV25 (likely *Caproiciproducens galactitolivorans*) (Figures 4 and 5, Figures S7, S8 and S14, Table S9).

For both bioreactors, the H_2 and CO_2-based CE phases (days 18–32 for R1 and days 23–42 for R2) were dominated by the *Megasphaera* genus, with relative abundances of 67% ± 23% for R1 and 79% ± 13% for R2 (Figures S7 and S8). ASV1 and ASV2 were the dominant species during these H_2 and CO_2-based CE phases (Figures 4 and 5). In bioreactor 1, the *Megasphaera* genus was overwhelmingly represented by ASV1 (likely *M. hexanoica*). In contrast, bioreactor 2 underwent a succession of *Megasphaera* species during the autotrophic H_2- and CO_2-based CE phase (Figures 4 and 5). Specifically, ASV2, 27 and 30 (likely *M. elsdenii*) dominated from day 25 to 32 (52% ± 12%), followed by ASV1 (likely *M. hexanoica*) until day 42 (86% ± 8%) before declining. Their decline marks the end of the H_2 and CO_2-based CE phase (Figures 4 and 5).

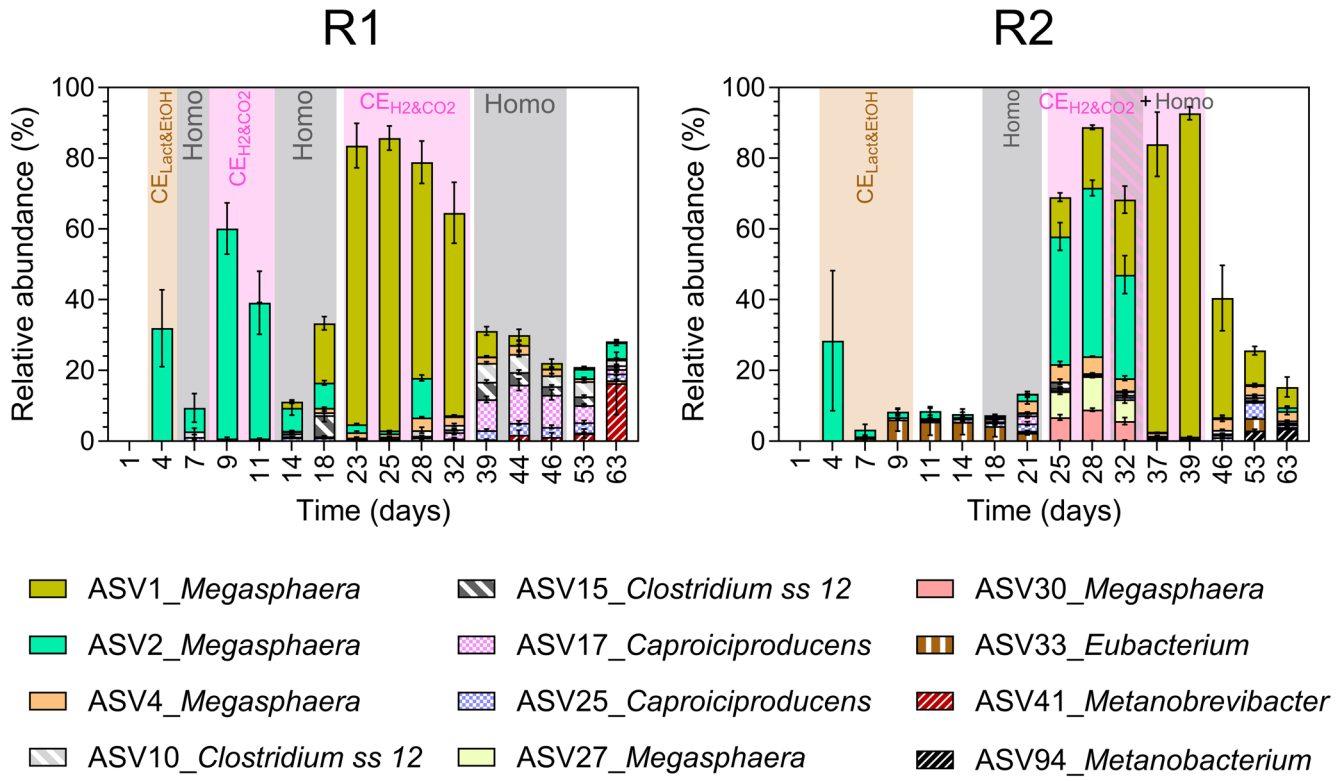

FIGURE 5 | The relative abundance of the 12 key ASVs associated with chain elongation (brown and pink patterns) and homoacetogenic (grey patterns) main metabolic phases identified during the fermentation for R1 (left) and R2 (right). Errors bars correspond to the standard deviation of the 3 technical replicates of each biological sample. "SS 12" indicates *sensu stricto* 12.

In bioreactor 1, homoacetogenic phases occurred before and after the autotrophic H_2- and CO_2-based CE phase, while in bioreactor 2, homoacetogenic phases occurred before and during the autotrophic H_2- and CO_2-based CE phase (Figure 1). Compared to the other metabolic phases, the top 10 significant taxa identified during the homoacetogenic phases comprised ASV17 and ASV25 (likely *Caproiciproducens galactitolivorans*), ASV15 (likely *C. luticellarii*), and ASV4 (likely *M. paucivorans*) (Figure S13F, Table S9). The heatmap (Figure 4) clustered both vertically and horizontally, ASVs 10, 17, 15, 25 and 4 together, showing their co-occurrence during the autotrophic period. All these taxa linked to both autotrophic homoacetogenic and H_2&CO_2-based CE phases showed low relative abundances that varied over time (Figure 5). The "Supplementary Spreadsheet, RelAb Dynamics" can be used to track the dynamics of all identified taxa.

The autotrophic period in both bioreactors ended with a methanogenic phase, involving different genera: *Methanobrevibacter* in R1 and *Methanobacterium* in R2, both being hydrogenotrophic methanogens. The development of these *Archaea* can be explained by their presence in the endogenous inoculum (Supporting Information Spreadsheet, "RelAb Dynamics"). It is hypothesized that they outcompeted the homoacetogens and the H_2-and CO_2-based chain elongators at the end of the fermentation, when nutrient and substrate availability was limited, allowing the slower-growing *Archaea* to develop. In bioreactor 1, ASV41 (likely *Methanobrevibacter aggregans*) was presumed to be responsible for methane production, while in bioreactor 2, ASV94 (likely *Methanobacterium acidilurans*) was the primary methanogen (Figure 5, Supporting Information Spreadsheet, "RelAb Dynamics").

3.2.3 | Correlation Between Metabolite Production Rate and Relevant ASVs

All absolute ASV abundances were clr-transformed, representing log-ratios relative to the community geometric mean. Figure 6 illustrates the correlation between clr-transformed abundances of significant ASVs (see Section 3.2.2) and average time-interval productivities (mol m^{-3}_{ML} d^{-1}, normalized to the mixed liquor volume in m^{-3}_{ML}) throughout fermentation in both bioreactors. Positive Spearman's correlation coefficients (in red, Figure 6) indicate a direct relationship between increases in ASV abundance and metabolite production rates. False-positive correlations may occur when the clr-transformed abundance of an ASV decreases while metabolites are being consumed. In contrast, negative Spearman's correlation coefficients (shown in blue, Figure 6) indicate an increase in ASV abundance associated with metabolite consumption, whereas false-negative correlations can appear when ASV abundance decreases while metabolites are produced. To minimize false positives and false negatives, only significant Spearman's correlation coefficients with a $p < 0.05$ are discussed below.

ASVs 1, 2 and 4 (likely *M. hexanoica*, *M. elsdenii* and *M. sueciensis*), ASVs 10 and 15 (likely *C. ljungdahlii* and *C. luticellarii*) and ASVs 17 and 25 (likely *Caproiciproducens galactitolivorans*) show significant correlations with the consumption of both H_2 and CO_2. Moreover, ASV1 (likely *M. hexanoica*) is also significantly correlated with the consumption of SCC (C2, C3, C4, C5) and the production of MCC (C6, C7 and C8). The three ASVs likely associated with *M. elsdenii* (ASVs 2, 27, and 30) exhibit

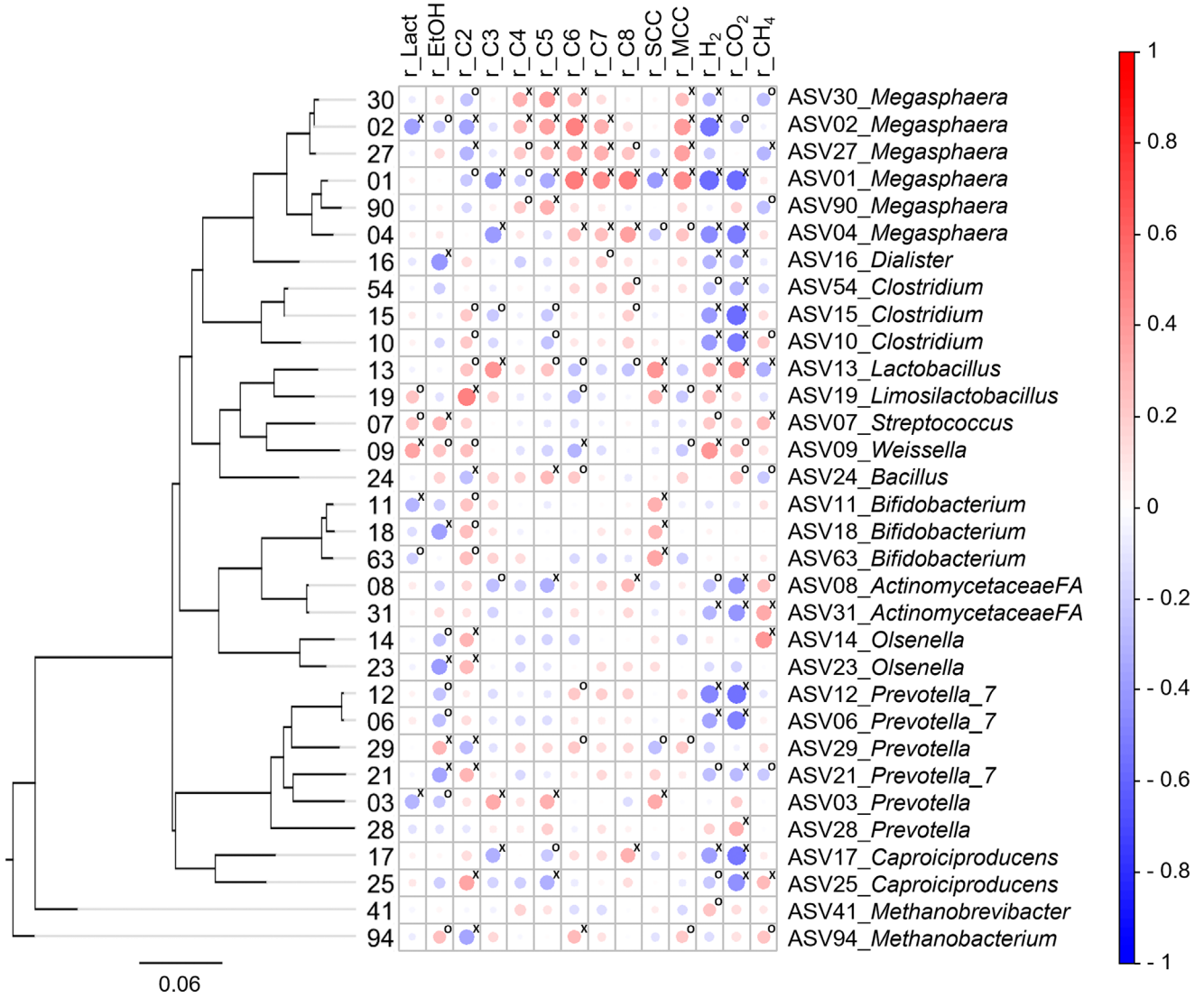

FIGURE 6 | Spearman correlation analysis between 32 significant ASVs across the entire fermentation process and metabolite production or consumption rates, r_i ($mole_i\ m^{-3}\ d^{-1}$), where i represents the metabolites shown on the top x-axis, from lactate to methane. All ASV abundances were clr-transformed prior to analysis. Significant correlations with a p-value below 0.01 are marked with an "X", while those with a p-value between 0.01 and 0.05 are marked with an "O". The 32 ASVs are grouped based on their phylogenetic tree (left) and are linked to their closest matching species, as determined by BLASTn analysis (right). Colour intensity represents the strength of the correlation, as measured by Spearman's rank correlation coefficients. Positive correlations (red) indicate that higher ASV abundance is associated with increased metabolite production rate, while negative correlations (blue) suggest that higher ASV abundance corresponds to increased metabolite consumption rate.

significant correlations with different metabolites. Specifically, ASV2 correlated with the consumption of lactate, H_2, CO_2, and C2, along with the production of carboxylates from C4 to C7. While ASVs 27 and 30 both showed significant correlation with C2 consumption, ASV30 is primarily associated with H_2 consumption and the production of C4, C5 and C6, whereas ASV27 mainly correlates with the production of C4 to C8, without significant H_2 and CO_2 consumption. ASV4 (likely *M. sueciensis*) correlates with the consumption of C3, H_2, and CO_2 and the production of C6 to C8. ASV10 (likely *C. ljungdahlii*), ASV15 and ASV 54 (likely *C. luticellarii*) and ASV25 (likely *C. galactitolivorans*) are significantly associated with the consumption of H_2 and CO_2 and the production of C2. Additionally, ASV17 (likely *C. galactitolivorans*), ASV15 and ASV54 (likely *C. luticellarii*) both significantly correlate with the consumption of H_2 and CO_2 and the production of C8.

4 | Discussion

4.1 | Microbiome Structure–Function Coupling During the Fermentation

4.1.1 | Megasphaera as a Versatile Consumer of Carbon and Electron Sources in Chain Elongation

The *Megasphaera* genus was identified as a key player in both bioreactors, with an average relative abundance of 56% ± 32% during all chain elongation phases, utilizing lactate, ethanol, or H_2 and CO_2. Distinct *Megasphaera*-associated ASVs emerged sequentially, each correlating with specific metabolite consumption and production (Figure 6). The predominant *Megasphaera* spp. exhibited phase-dependent dynamics: ASVs 2, 27, and 30 (likely *M. elsdenii*) persisted in both mixotrophic

and autotrophic conditions, while ASV1 (likely *M. hexanoica*) dominated during autotrophy. Figure 7 illustrates metabolite production kinetics alongside the *Megasphaera* spp. relative abundance and the relative abundances shift of ASV1 (likely *M. hexanoica*) and ASV2 (likely *M. elsdenii*) throughout the chain elongation process.

4.1.2 | ASV2 (Likely *M. elsdenii*) as a Carboxylate (SCC and MCC) Producer From Lactate

ASV2 (likely *M. elsdenii*) is notably prevalent during the EtOH- and lactate-based chain elongation phases (Figure 7, Table S9, Figure S13C), with an average relative abundance of 30% ± 14% on day 4 in R1 and R2 (representing over 98% of all *Megasphaera*-associated reads) (Figure 7). This time point coincides with lactate consumption in both reactors (Figure 1), while ethanol is being produced (Figure 7). *M. elsdenii* is known to metabolize lactate into various SCC and MCC, including C2, C3, C4, C5, and C6 (Chen et al. 2019; Prabhu et al. 2012; Weimer and Moen 2013). The significant negative Spearman coefficient between ASV2 and lactate (Figure 6), indicates that ASV2 is a key lactate-utilizing species in this system. Since the other lactate consumers, such as *Bifidobacterium* spp. (ASVs 11 and 63) and ASV3 (likely *Segatella paludivivens*) (Figure 6), do not produce MCC, ASV2 (likely *M. elsdenii*) becomes the only taxon responsible for MCC production from lactate during this fermentation phase (see Section 4.1.6 for a discussion on other lactate utilizers).

4.1.3 | Is ASV2 (Likely *M. elsdenii*) a Chain Elongator From H_2, CO_2, Acetate, and Propionate?

In both bioreactors, alongside MCC production, the relative abundance of ASV2 (likely *M. elsdenii*) increased a second time

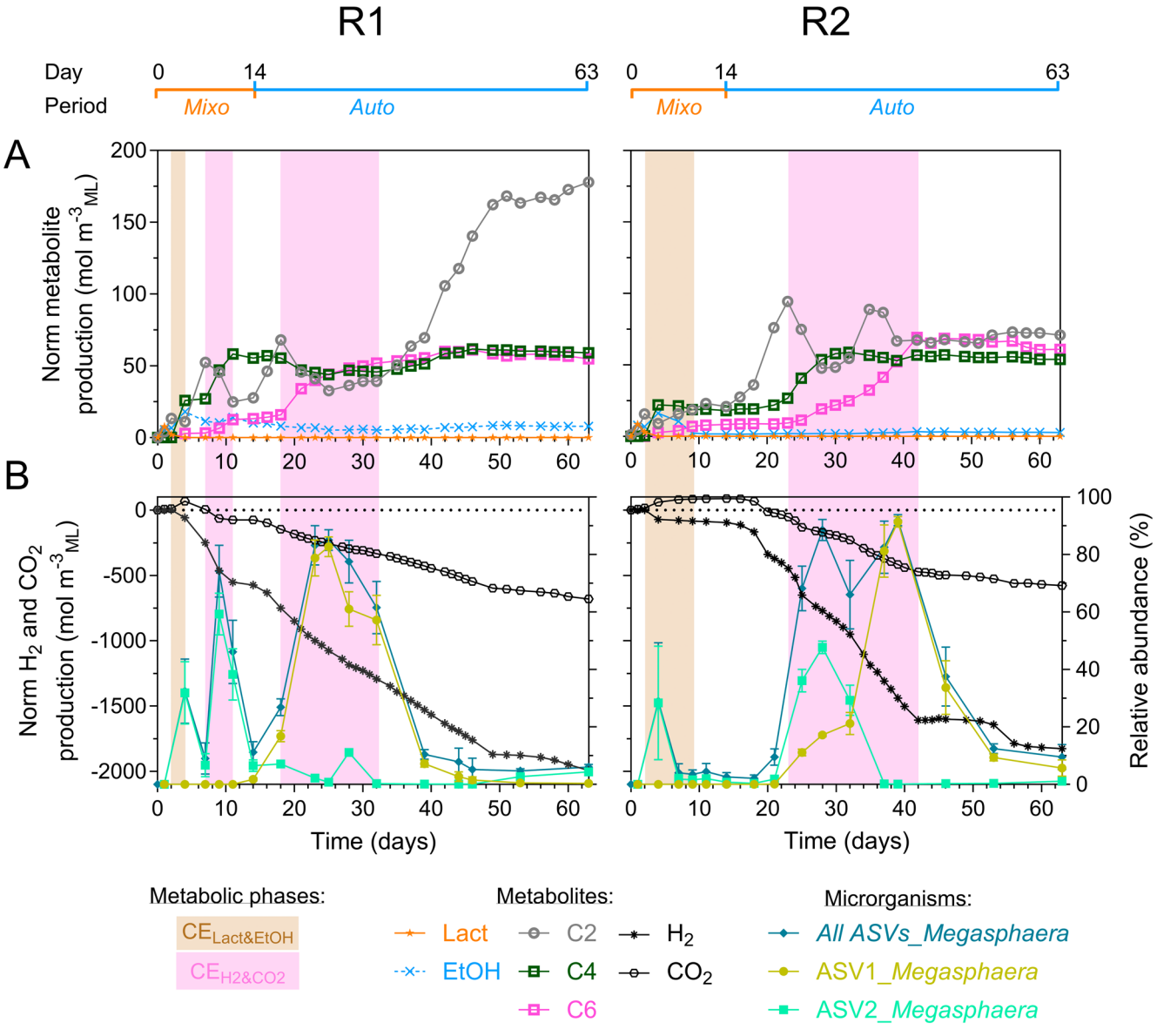

FIGURE 7 | Cumulative soluble (A) and gaseous (B) metabolite production, normalized to the mixed liquor volume (in m^3_{ML}), over the 63-day fermentation in reactor 1 (R1, left) and reactor 2 (R2, right). The relative abundances of ASV 1 and ASV 2 are shown in panel B with gas monitoring. Brown shading indicates ethanol- and lactate-based chain elongation, while pink shading marks H_2- and CO_2-based CE.

reaching an average relative abundance of 49% ± 14% in bioreactor 1 from day 9 to day 11, and 38% ± 9% in bioreactor 2 from day 25 to day 32 (Figures 1, 5 and 7). These resurgences were observed in both bioreactors during an H_2- and CO_2-based CE phase, coinciding with the mixotrophic period in bioreactor 1 and the autotrophic period in bioreactor 2.

M. elsdenii is known to convert carbohydrates (mainly glucose) or lignocellulosic hydrolysates into carboxylates (C2, C3, C4, C5, and C6) (Weimer and Moen 2013; Nelson et al. 2017). In bioreactor 1, the presence of the fermentable fraction of BSG that had not yet been fully converted may explain *M. elsdenii* resurgence during the mixotrophic H_2- and CO_2-based CE phase (days 9–11). However, in bioreactor 2, the fermentable fraction of BSG had been largely depleted during the autotrophic H_2- and CO_2-based CE phase (days 25–32), which cannot explain the reappearance of ASV2 (Figure 7). In addition, according to known metabolic pathways, acetate, H_2, and CO_2 should have been produced if carbohydrates or lactate were used as electron donors and carbon sources for chain elongation (da S. Cabral and Weimer 2024), whereas in both bioreactors during these intervals, acetate, H_2, and CO_2 were intensely consumed (Figure 7). Indeed, from day 25 to day 32 in bioreactor 2, the microbiome, dominated by ASV2 (likely *M. elsdenii*), consumed acetate, H_2, and CO_2 to produce butyrate, valerate, caproate, and heptanoate (Figures 1 and 7). The consumption of acetate, H_2, and CO_2, along with the production of C4, C5, C6, and C7, is strongly correlated with the presence of ASV2 (likely *M. elsdenii*) (Figure 6). Moreover, *M. elsdenii*-associated ASVs 27 and 30 showed similar correlations with acetate and H_2 consumption and with the production of C4, C5, and MCC (Figure 6). This suggests that *M. elsdenii* plays a key role in the elongation of carboxylates, regardless of the initial carboxylate chain length or whether it contains an even or odd number of carbons.

In addition to *M. elsdenii* significantly consuming SCC, its negative correlation with H_2 and CO_2 production rates suggests a potential to consume these gases (Figure 6). The consumption of H_2 correlates significantly with ASV2 and ASV30 ($p < 0.01$, Figure 6), and almost significantly with ASV27 ($p = 0.053$). Interestingly, CO_2 consumption correlates only with ASV2 ($p < 0.05$, Figure 6). Since these three *M. elsdenii* ASVs accounts for 52% ± 12% of the microbial community in bioreactor 2 from day 25 to 32, and the electron and carbon balances (Figure S3) indicates that 82%–85% of supplied H_2 and 83%–86% of supplied CO_2 are incorporated into metabolites during the autotrophic period, *M. elsdenii* most likely utilizes both H_2 and CO_2 in its chain elongation pathway. Additionally, syntrophic, or synergistic interactions between homoacetogens and *M. elsdenii* may explain elongated carboxylates production alongside H_2 and CO_2 consumption (Section 4.2).

4.1.4 | Is ASV1 (Likely *M. hexanoica*) the Specialist in MCC Production From SCC, H_2 and CO_2?

In both bioreactors, ASV1 (likely *M. hexanoica*) dominates the autotrophic period showing an overwhelming relative abundance during H_2 and CO_2-based CE phases up to 91% ± 2% in bioreactor 1 and 83% ± 3% in bioreactor 2 (Figures 5 and 7, Supporting Information Spreadsheet, RelAb Dynamics). Figure 6 shows that ASV1 (likely *M. hexanoica*) significantly consumes H_2, CO_2, SCC (C2, C3, C4 and C5) and significantly produces MCC (C6, C7 and C8). During H_2 and CO_2-based CE phases, the fermentable fraction of BSG was nearly depleted, with no detected consumption of lactate or ethanol, leaving H_2 as the sole available reducing equivalent. Compared to *M. elsdenii* ASVs, ASV1 (likely *M. hexanoica*) correlates more strongly with H_2, CO_2, C4, and C5 consumption (Figure 6), suggesting ASV1 (likely *M. hexanoica*) is the specialist producer of MCC in this system. The proposed pathway for MCC production by *M. hexanoica* from H_2, CO_2, and carboxylates is discussed in Section 4.3.

4.1.5 | Homoacetogens as Key Players in Mixotrophic Chain Elongation System

In both bioreactors, multiple homoacetogenic phases, characterized by acetate production and H_2&CO_2 consumption, occurred during mixotrophic and autotrophic periods (Figure 1). ASVs 10, 15, 17 and 25 (likely *C. ljungdahlii*, *C. luticellarii* and *Caproiciproducens galactitolivorans*) cluster in the dendrogram during the autotrophic homoacetogenic phases (Figure 4) and are statistically significant during autotrophic homoacetogenic phases compared to the other metabolic phases (Figure S13F, Table S9). Moreover, all three correlate significantly with H_2 and CO_2 consumption and acetate production (Figure 6).

C. ljungdahlii is a well-established acetogen that produces acetate from H_2 and CO_2, among other substrates (Hermann et al. 2020; Tanner et al. 1993; Köpke et al. 2010). *C. luticellarii* has recently been identified as a major producer of acetic acid at pH 6.5 in the presence of H_2 and CO_2 (Mariën et al. 2023). Despite their low relative abundance during acetate-producing phases, *C. ljungdahlii* (ASV10, 2.3% ± 2.1%) and *C. luticellarii* (ASV15, 2.6% ± 2.2%) seem to be the main acetate producers. With a calculated soluble concentration of H_2 and CO_2 oscillating from 0.59 to 0.69 mM_{H2} and from 6.59 to 7.75 mM_{CO2}, and a measured pH oscillating from 6 to 6.8 for both bioreactors, these (homo-)acetogens from the *Clostridiaceae* family are in the right condition to grow (Poehlein et al. 2025; Laura and Jo 2023).

In contrast, the significant presence of ASV17 and ASV25 (likely *Caproiciproducens galactitolivorans*) during homoacetogenic phases is unexpected (Figure S13F, Table S9). Indeed, this species is closely related to *Caproicibacter fermentans*, known for producing carboxylates, H_2 and CO_2 from carbohydrates (Kim et al. 2015; Flaiz et al. 2020). Its identification as a significant taxon throughout the autotrophic period seems inconsistent (Table S9). A plausible hypothesis is that this species gradually metabolizes the residual solid fraction of BSG, which slowly solubilizes over time. This aligns with incomplete electron and carbon balances observed during the autotrophic period (Figure S3), suggesting forgotten processes and additional electron and carbon inputs to close these balances (Heijnen and Verheijen 2011).

4.1.6 | Supporting and Competing Taxa Involved in Chain Elongation Process

During the mixotrophic period, *Olsenella*, *Lactobacillus*, *Limosilactobacillus*, *Bifidobacterium*, *Prevotella*, and *Prevotella_7* are

identified as SCC-producing genera (Figure 6). *Limosillactobacillus*, *Streptococcus*, and *Weissella* genera appear to be the main lactate producers, as their representative ASVs (respectively 19, 7 and 9) show significant positive coefficients in the Spearman correlation analysis (Figure 6). In contrast, ASV 3 (likely *Segatella paludivivens*) and ASVs 11 and 63 (*Bifidobacterium* spp.) seem to significantly consume lactate for SCC production (Figure 6). Interestingly, *S. paludivivens* is not known to metabolize lactate and instead produces acetate from carbohydrates (Hitch et al. 2022; Ueki et al. 2007). Similarly, *Bifidobacterium* spp. are reported not to metabolize lactate (Mattarelli 2018), though they produce it along with acetate via hexose and pentose fermentation (Spormann 2023). Since lactate consumption and carbohydrate conversion can occur simultaneously but through distinct metabolic pathways, Spearman's correlations should be interpreted cautiously, as they may reflect co-occurrence rather than direct metabolic interactions.

These results also suggest that ASV2 (likely *M. elsdenii*) is the only significant lactate utilizer in the system (Figure 6). Its co-occurrence with lactate producers indicates cross-feeding activity among these genera. Zhao et al. (2024) recently demonstrated lactate cross-feeding between *Bifidobacterium* spp. and *Megasphaera indica*, contributing to butyrate production in the human colon. In the present system, lactic acid producing bacteria, such as *Bifidobacterium*, *Limosillactobacillus*, *Weissella*, and *Bacillus* likely support the growth of *M. elsdenii*, enabling carboxylate production, primarily butyrate and caproate.

ASV33, mainly detected in bioreactor 2, was identified as *Eubacterium* [nodatum group], closely related to *Aminicella lysinolytica or Eubacterium pyruvativorans* (Figure 5). Both species are non-saccharolytic bacteria but ferment amino acids to produce carboxylates (Wallace et al. 2003, 2004; Ueki et al. 2015). Another carboxylate-producing, amino-acid-fermenting anaerobe, *Acidaminococcus fermentans* (ASV34), was predominant during the first 25 days in both bioreactors (Supporting Information Spreadsheet, "RelAb Dynamics"). This suggests that BSG protein degradation, previously reported by Henry et al. (2023), likely occurred in this experiment, with these proteins being partially converted into carboxylates.

During methanogenic phases, ASV41 (likely *Methanobrevibacter acididurans*) and ASV94 (likely *Methanobacterium aggregans*) are identified as the primary contributors to methane production. Both *Methanobrevibacter* and *Methanobacterium* are hydrogenotrophic methanogens (Boone 2015; Miller 2015), accounting for 79% and 21% of all *Archaea* detected during the entire fermentation, respectively. The absence of acetate consumption and aceticlastic methanogens during the methanogenic phases suggests that aceticlastic methanogenesis is being inhibited. This is probably due to the high partial pressure of H_2, which is preventing the growth of their required syntrophic fatty acid oxidizers (Schink 1997).

4.2 | Proposed MCC Production Pathway in This System

Figure 8 illustrates microbial interactions during mixotrophic and autotrophic periods. In addition to acidogenic bacteria metabolizing BSG into intermediates and homoacetogenic bacteria converting H_2 and CO_2 into acetate, our findings indicate that *Megasphaera* spp. are the primary chain elongators in this mixed culture fermentation. ASV2 (likely *M. elsdenii*) appears to be a versatile chain elongator, consuming lactate, H_2, CO_2, and C2 to produce SCC and MCC (C4 to C7). In contrast, ASV1 (likely *M. hexanoica*) appears to be a more specialized MCC producer in this system by consuming H_2, CO_2, and C2–C5 to generate C6–C8. The co-occurrence of *Megasphaera* spp. with ASV10 and ASV15 (likely *C. ljungdahlii* and *C. luticellarii*) suggests potential syntrophic/synergistic interactions. Mook et al. (2024) recently reported on the interaction between an engineered *Acetobacterium woodii* that consumes H_2 and CO_2 to produce lactate, and a *Clostridium drakei* strain SL1 that generated elongated carboxylates from that lactate. In the present work, homoacetogens ASVs 10 and 15 (likely *C. ljungdahlii* and *C. luticellarii*) may produce acetate from H_2 and CO_2, while *Megasphaera* spp. consume acetate in combination with H_2 and CO_2 to produce elongated carboxylates.

4.3 | Hypothetical Direct Use of CO_2 and H_2 by *Megasphaera* spp.

To our knowledge, this is the first report associating *Megasphaera* spp. (presumably *M. elsdenii* and *M. hexanoica*) with the consumption of H_2, CO_2 and SCC to produce elongated carboxylates. However, *M. elsdenii* was already reported to utilize H_2 in 1953 (Elsden and Lewis 1953). In their preliminary study, Elsden and Lewis (1953) identified bacterial strain LC, later confirmed as *M. elsdenii*, as capable of using gaseous H_2 during pyruvate fermentation to produce carboxylates. They also found that adding C2, C3 or C4 during pyruvate fermentation enhanced H_2 consumption and increased the formation of C4, C5 and C6, respectively (Elsden and Lewis 1953). However, these experiments were conducted under low CO_2 partial pressure, limiting their ability to assess CO_2 uptake.

More recently, Lee et al. (2020) conducted a genome-scale metabolic network reconstruction, suggesting that *M. elsdenii* can fix CO_2 to produce butyrate and caproate. The proposed pathway combines an incomplete reductive tricarboxylic acid cycle (rTCA) with a subsequent RBO cycle (Lee et al. 2020). The pathway starts from pyruvate and HCO_3^-, where ATP-dependent pyruvate carboxylase generates oxaloacetate, which continues through the rTCA to crotonyl-CoA. Crotonyl-CoA is then converted to butyryl-CoA, which can either form butyrate or enter the RBO cycle as butyryl-CoA, ultimately yielding caproate (Kim et al. 2022; Lee et al. 2020). Taken together, this study shows *M. elsdenii* and *M. hexanoica* may directly metabolize SCC, H_2 and CO_2 to produce elongated carboxylates, without synergic or syntrophic interactions with other functional groups. This would be possible only if (i) pyruvate can be generated from H_2 and CO_2, and (ii) H_2 can serve directly as a reducing equivalent.

Pyruvate can be produced from acetyl-CoA and CO_2. Under high CO_2 partial pressure, the TCA cycle can reverse towards autotrophy, converting acetyl-CoA and CO_2 to pyruvate by reductive carboxylation catalysed by pyruvate synthase, without ATP requirement (Steffens et al. 2021; Berg 2011). The observed consumption of H_2 could be directly catalysed by

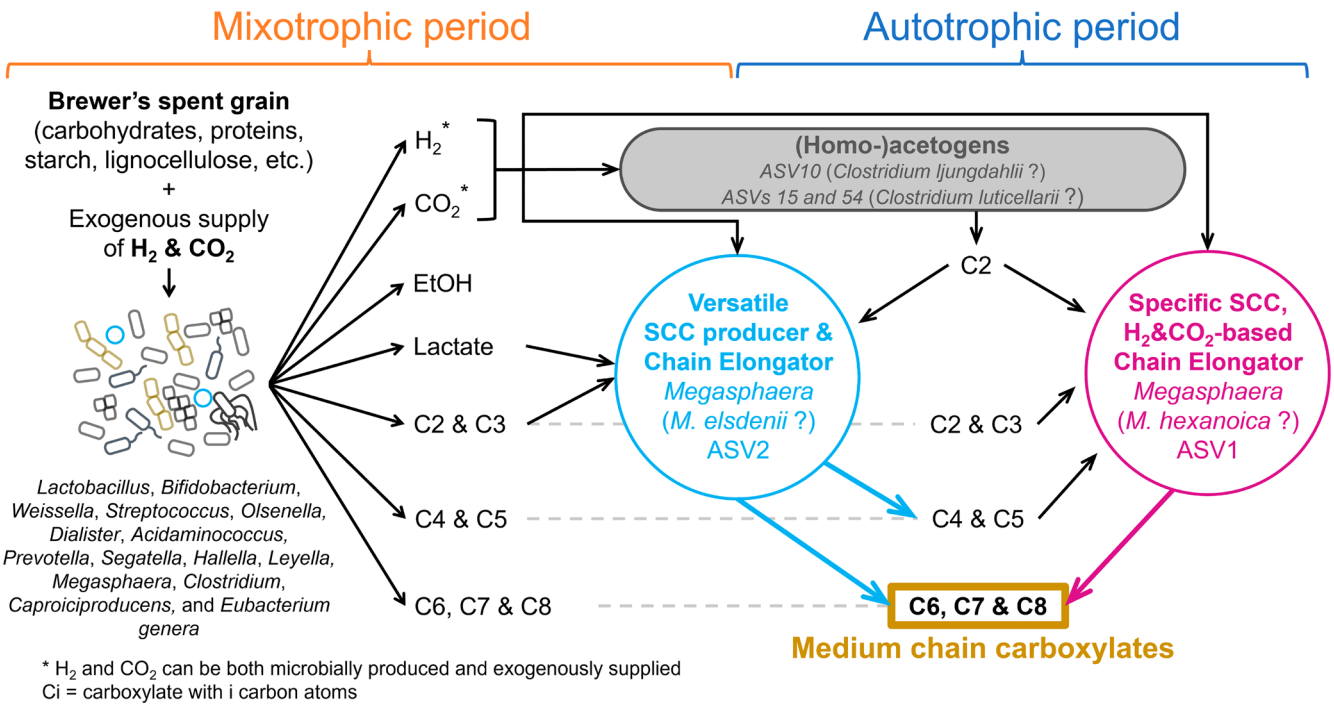

FIGURE 8 | Proposed microbial interactions during mixotrophic and the autotrophic BSG fermentation in the presence of H_2 and CO_2.

Megasphaera spp. through their hydrogenases. *M. elsdenii* has genes encoding different types of hydrogenases (Van Dijk et al. 1979; Atta and Meyer 2000; Caserta et al. 2016). While hydrogenases, such as Hyd (Esselborn et al. 2013; Katsyv et al. 2023), are mainly studied for H_2 generation, they can also catalyse the oxidation of H_2 into protons and electrons (Fourmond et al. 2021). In the oxidation mode, hydrogenases generate electrons that contribute to the respiratory chain for ATP production. Additionally, some soluble hydrogenases can regenerate reduced cofactors NAD(P)H by consuming supplied H_2 (Lubitz et al. 2014). For chain elongation, reduced NADH is essential for driving the reverse β-oxidation, with 2 mol of NADH required per elongation cycle (Wu et al. 2017). Similarly, the production of crotonyl-CoA from pyruvate via the reductive TCA requires 4 mol of NADH (Kim et al. 2022).

Although *Megasphaera* spp. possess hydrogenases for H_2 metabolism and *M. elsdenii* can utilize CO_2 through a partial reductive TCA cycle, the pathway to produce elongated carboxylates from H_2, CO_2, and carboxylates remains unclear. In addition, the significant decline in the relative abundance of *Megasphaera*, along with the sharp decrease in elongated carboxylate production (Figures 1 and 7), indicates that the conditions required to sustain elongated carboxylate production using SCC, H_2 and CO_2 have not yet been fully optimized. These decreases in abundance and production may suggest inhibition from carboxylate toxicity (Jarboe et al. 2013; Desbois and Smith 2010), nutrient deficiencies, unfavourable growth conditions, or competing pathways consuming H_2 and CO_2. Further studies should focus on the eco-physiology of *M. elsdenii* and *M. hexanoica* to identify their specific MCC production pathways using carboxylates, H_2, and CO_2, and to assess the impacts of carboxylate concentrations and other limiting nutrients on growth.

5 | Conclusion

This study identifies *Megasphaera* spp. (presumably *Megasphaera elsdenii* and *Megasphaera hexanoica*) as the primary species responsible for MCC production in a mixed culture fermentation system fed by a combination of organic (brewer's spent grain) and inorganic (H_2 and CO_2) substrates. ASV 2 (likely *Megasphaera elsdenii*) is identified as a versatile chain elongator, capable of producing both SCC and MCC from lactate in the early fermentation phases, and elongated carboxylates (mainly butyrate, valerate and caproate) from acetate, propionate, H_2 and CO_2. Under the investigated conditions, ASV1 (likely *M. hexanoica*) appears to be specifically adapted to produce MCC (caproate, heptanoate and octanoate) from H_2, CO_2 and SCC (acetate, propionate, butyrate and valerate), primarily during the autotrophic period. Potential syntrophic or synergistic interactions between acetogens from the *Clostridiaceae* family (presumably *C. ljungdahlii* and *C. luticellarii*) with *Megasphaera* spp. are suggested by the formation and utilization of acetate during the mixotrophic and autotrophic H_2- and CO_2-based CE phases. This study is the first one to suggest that *Megasphaera* spp. can directly use H_2 and CO_2 along with carboxylates to produce elongated carboxylates, enhancing the targeted production of medium-chain carboxylates. Further studies on pure or polycultures of *M. elsdenii* and *M. hexanoica* in H_2 and CO_2 environments, with or without carboxylate supplementation, and with or without the identified homoacetogens (likely *C. ljungdahlii* and *C. luticellarii*), could provide valuable insights into the MCC production pathway in this system.

Author Contributions

G. B. L. Henry: conceptualization, investigation, methodology, validation, visualization, writing – original draft preparation. J. Tremblay: resources, formal analysis, software, writing – review and editing. B. A. Stenuit: supervision, methodology, formal analysis, software, visualization, data curation, writing – review and editing. P. A. Gerin: supervision, project administration, funding acquisition, writing – review and editing.

Acknowledgements

This work was possible owing to the combination of funding by Service Public de Wallonie through the eBIO2CHEM project, co-funding of the European Union and Région Wallonne (FEDER, see https://europe.wallonie.be/ or https://www.enmieux.be/) through the ENERBIO project, and Région de Bruxelles Capitale/INNOVIRIS through the Re4Bru project. The authors thankfully acknowledge Arnaud Isenborghs, Simon Van Laethem, Antoine de Halloy de Waulsort for their help in monitoring the bioreactors, Thomas Nicolay for the coding of the excel sheet for raw data analysis, and the MOCA platform of UCLouvain with Matthieu Leclercq and Hélène Dailly for their valuable contribution to the metabolites analyses by gas and liquid chromatography. The Bertinchamps craft brewery in Gembloux is also gratefully acknowledged for providing the brewer's spent grain used in this study.

Funding

This work was supported by Service Public de Wallonie, SPW-DGO3-D65-1454, SPW-DGO3-D31-1397; Région de Bruxelles-Capitale, 2019-BRIDGE-4D; European Regional Development Fund.

Conflicts of Interest

The authors declare no conflicts of interest.

Data Availability Statement

Amplicon sequence raw data is available on the NCBI's portal as accession identifier PRJNA1222319. Data are available in article Supporting Information. Fermentation raw data are available upon request from the author.

References

Agler, M. T., C. M. Spirito, J. G. Usack, J. J. Werner, and L. T. Angenent. 2012. "Chain Elongation With Reactor Microbiomes: Upgrading Dilute Ethanol to Medium-Chain Carboxylates." *Energy & Environmental Science* 5: 8189. https://doi.org/10.1039/c2ee22101b.

Angenent, L. T., H. Richter, W. Buckel, et al. 2016. "Chain Elongation With Reactor Microbiomes: Open-Culture Biotechnology to Produce Biochemicals." *Environmental Science & Technology* 50: 2796–2810. https://doi.org/10.1021/acs.est.5b04847.

Atta, M., and J. Meyer. 2000. "Characterization of the Gene Encoding the [Fe]-Hydrogenase From *Megasphaera elsdenii*." *Biochimica et Biophysica Acta (BBA)—Protein Structure and Molecular Enzymology* 1476: 368–371. https://doi.org/10.1016/S0167-4838(99)00245-9.

Baleeiro, F. C. F., S. Kleinsteuber, A. Neumann, and H. Sträuber. 2019. "Syngas-Aided Anaerobic Fermentation for Medium-Chain Carboxylate and Alcohol Production: The Case for Microbial Communities." *Applied Microbiology and Biotechnology* 103: 8689–8709. https://doi.org/10.1007/s00253-019-10086-9.

Baleeiro, F. C. F., S. Kleinsteuber, and H. Sträuber. 2021. "Hydrogen as a Co-Electron Donor for Chain Elongation With Complex Communities." *Frontiers in Bioengineering and Biotechnology* 9: 650631. https://doi.org/10.3389/fbioe.2021.650631.

Baleeiro, F. C. F., J. Raab, S. Kleinsteuber, A. Neumann, and H. Sträuber. 2022. "Mixotrophic Chain Elongation With Syngas and Lactate as Electron Donors." *Microbial Biotechnology* 16: 1751–7915. https://doi.org/10.1111/1751-7915.14163.

Baleeiro, F. C. F., L. Varchmin, S. Kleinsteuber, H. Sträuber, and A. Neumann. 2023. "Formate-Induced CO Tolerance and Methanogenesis Inhibition in Fermentation of Syngas and Plant Biomass for Carboxylate Production." *Biotechnology for Biofuels and Bioproducts* 16: 26. https://doi.org/10.1186/s13068-023-02271-w.

Batlle-Vilanova, P., R. Ganigué, S. Ramió-Pujol, et al. 2017. "Microbial Electrosynthesis of Butyrate From Carbon Dioxide: Production and Extraction." *Bioelectrochemistry* 117: 57–64. https://doi.org/10.1016/j.bioelechem.2017.06.004.

Bengelsdorf, F. R., M. H. Beck, C. Erz, et al. 2018. "Chapter Four—Bacterial Anaerobic Synthesis Gas (Syngas) and CO_2 + H_2 Fermentation." In *Advances in Applied Microbiology*, 143–221. Elsevier. https://doi.org/10.1016/bs.aambs.2018.01.002.

Bengelsdorf, F. R., and P. Dürre. 2017. "Gas Fermentation for Commodity Chemicals and Fuels." *Microbial Biotechnology* 10: 1167–1170. https://doi.org/10.1111/1751-7915.12763.

Berg, I. A. 2011. "Ecological Aspects of the Distribution of Different Autotrophic CO_2 Fixation Pathways." *Applied and Environmental Microbiology* 77: 1925–1936. https://doi.org/10.1128/AEM.02473-10.

Bianco, A., G. Zara, M. Garau, et al. 2024. "Microbial Community Assembly and Chemical Dynamics of Raw Brewers' Spent Grain During Inoculated and Spontaneous Solid-State Fermentation." *Waste Management* 174: 518–527. https://doi.org/10.1016/j.wasman.2023.12.021.

Boone, D. R. 2015. "Methanobacterium." In *Bergey's Manual of Systematics of Archaea and Bacteria*, edited by W. B. Whitman, 1st ed., 1–8. Wiley. https://doi.org/10.1002/9781118960608.gbm00495.

Cabau-Peinado, O., A. J. J. Straathof, and L. Jourdin. 2021. "A General Model for Biofilm-Driven Microbial Electrosynthesis of Carboxylates From CO_2." *Frontiers in Microbiology* 12: 669218. https://doi.org/10.3389/fmicb.2021.669218.

Carvalheira, M., C. L. Amorim, A. C. Oliveira, et al. 2022. "Valorization of Brewery Waste Through Polyhydroxyalkanoates Production Supported by a Metabolic Specialized Microbiome." *Life* 12: 1347. https://doi.org/10.3390/life12091347.

Caserta, G., A. Adamska-Venkatesh, L. Pecqueur, et al. 2016. "Chemical Assembly of Multiple Metal Cofactors: The Heterologously Expressed Multidomain [FeFe]-Hydrogenase From *Megasphaera elsdenii*." *Biochimica et Biophysica Acta, Bioenergetics* 1857: 1734–1740. https://doi.org/10.1016/j.bbabio.2016.07.002.

Chen, L., Y. Shen, C. Wang, et al. 2019. "*Megasphaera elsdenii* Lactate Degradation Pattern Shifts in Rumen Acidosis Models." *Frontiers in Microbiology* 10: 162. https://doi.org/10.3389/fmicb.2019.00162.

Chen, W. S., Y. Ye, K. J. J. Steinbusch, D. P. B. T. B. Strik, and C. J. N. Buisman. 2016. "Methanol as an Alternative Electron Donor in Chain Elongation for Butyrate and Caproate Formation." *Biomass Bioenergy* 93: 201–208. https://doi.org/10.1016/j.biombioe.2016.07.008.

da S. Cabral, L., and P. J. Weimer. 2024. "*Megasphaera elsdenii*: Its Role in Ruminant Nutrition and Its Potential Industrial Application for Organic Acid Biosynthesis." *Microorganisms* 12: 219. https://doi.org/10.3390/microorganisms12010219.

De Groof, V., M. Coma, T. Arnot, D. J. Leak, and A. B. Lanham. 2021. "Selecting Fermentation Products for Food Waste Valorisation With HRT and OLR as the Key Operational Parameters." *Waste Management* 127: 80–89. https://doi.org/10.1016/j.wasman.2021.04.023.

Dellomonaco, C., J. M. Clomburg, E. N. Miller, and R. Gonzalez. 2011. "Engineered Reversal of the β-Oxidation Cycle for the Synthesis of

Fuels and Chemicals." *Nature* 476: 355–359. https://doi.org/10.1038/nature10333.

Desbois, A. P., and V. J. Smith. 2010. "Antibacterial Free Fatty Acids: Activities, Mechanisms of Action and Biotechnological Potential." *Applied Microbiology and Biotechnology* 85: 1629–1642. https://doi.org/10.1007/s00253-009-2355-3.

Dewhirst, F. E., B. J. Paster, N. Tzellas, et al. 2001. "Characterization of Novel Human Oral Isolates and Cloned 16S rDNA Sequences That Fall in the Family *Coriobacteriaceae*: Description of *Olsenella* Gen. Nov., Reclassification of *Lactobacillus uli* as *Olsenella uli* Comb. Nov. and Description of *Olsenella profusa* sp. Nov." *International Journal of Systematic and Evolutionary Microbiology* 51: 1797–1804. https://doi.org/10.1099/00207713-51-5-1797.

du Toit, M., M. Huch, G. Cho, and C. M. A. P. Franz. 2014. "The Genus *Streptococcus*." In *Lactic Acid Bacteria*, edited by W. H. Holzapfel and B. J. B. Wood, 1st ed., 457–505. Wiley. https://doi.org/10.1002/9781118655252.ch28.

Dufrêne, M., and P. Legendre. 1997. "Species Assemblages and Indicator Species: The Need for a Flexible Asymmetrical Approach." *Ecological Monographs* 67: 345–366. https://doi.org/10.1890/0012-9615(1997)067[0345:SAAIST]2.0.CO;2.

Edgar, R. C. 2018. "Updating the 97% Identity Threshold for 16S Ribosomal RNA OTUs." *Bioinformatics* 34: 2371–2375. https://doi.org/10.1093/bioinformatics/bty113.

Egan, M. 2018. "Chapter 8—Carbohydrate Metabolism in *Bifidobacteria*." In *The Bifidobacteria and Related Organisms: Biology, Taxonomy, Applications*, 145–164. Elsevier.

Elsden, S. R., and D. Lewis. 1953. "The Production of Fatty Acids by a Gram-Negative Coccus." *Biochemical Journal* 55: 183–189. https://doi.org/10.1042/bj0550183.

Esquivel-Elizondo, S., A. G. Delgado, and R. Krajmalnik-Brown. 2017. "Evolution of Microbial Communities Growing With Carbon Monoxide, Hydrogen, and Carbon Dioxide." *FEMS Microbiology Ecology* 93: fix076. https://doi.org/10.1093/femsec/fix076.

Esquivel-Elizondo, S., A. G. Delgado, B. E. Rittmann, and R. Krajmalnik-Brown. 2017. "The Effects of CO_2 and H_2 on CO Metabolism by Pure and Mixed Microbial Cultures." *Biotechnology for Biofuels* 10: 220. https://doi.org/10.1186/s13068-017-0910-1.

Esselborn, J., C. Lambertz, A. Adamska-Venkatesh, et al. 2013. "Spontaneous Activation of [FeFe]-Hydrogenases by an Inorganic [2Fe] Active Site Mimic." *Nature Chemical Biology* 9: 607–609. https://doi.org/10.1038/nchembio.1311.

Ferreira, S., E. Monteiro, P. Brito, C. Castro, L. Calado, and C. Vilarinho. 2019. "Experimental Analysis of Brewers' Spent Grains Steam Gasification in an Allothermal Batch Reactor." *Energies* 12: 912. https://doi.org/10.3390/en12050912.

Flaiz, M., T. Baur, S. Brahner, A. Poehlein, R. Daniel, and F. R. Bengelsdorf. 2020. "*Caproicibacter fermentans* Gen. Nov., sp. Nov., a New Caproate-Producing Bacterium and Emended Description of the Genus *Caproiciproducens*." *International Journal of Systematic and Evolutionary Microbiology* 70: 4269–4279. https://doi.org/10.1099/ijsem.0.004283.

Fourmond, V., N. Plumeré, and C. Léger. 2021. "Reversible Catalysis." *Nature Reviews Chemistry* 5: 348–360. https://doi.org/10.1038/s41570-021-00268-3.

Fusco, V., G. M. Quero, G.-S. Cho, et al. 2015. "The Genus *Weissella*: Taxonomy, Ecology and Biotechnological Potential." *Frontiers in Microbiology* 6: 155. https://doi.org/10.3389/fmicb.2015.00155.

Gemeinhardt, K., B. S. Jeon, J. N. Ntihuga, et al. 2025. "Toward Industrial C8 Production: Oxygen Intrusion Drives Renewable *n*-Caprylate Production From Ethanol and Acetate *via* Intermediate Metabolite Production." *Green Chemistry* 27: 2931–2949. https://doi.org/10.1039/D5GC00411J.

Grootscholten, T. I. M., F. Kinsky dal Borgo, H. V. M. Hamelers, and C. J. N. Buisman. 2013. "Promoting Chain Elongation in Mixed Culture Acidification Reactors by Addition of Ethanol." *Biomass Bioenergy* 48: 10–16. https://doi.org/10.1016/j.biombioe.2012.11.019.

Heijnen, S. J., and P. J. T. Verheijen. 2011. "How to Obtain True and Accurate Rate-Values." In *Methods in Enzymology*, 457–508. Elsevier. https://doi.org/10.1016/B978-0-12-385118-5.00023-2.

Henry, G. B. L., F. Awedem Wobiwo, A. Isenborghs, et al. 2023. "A Specific H_2/CO_2 Consumption Molar Ratio of 3 as a Signature for the Chain Elongation of Carboxylates From Brewer's Spent Grain Acidogenesis." *Frontiers in Bioengineering and Biotechnology* 11: 1165197. https://doi.org/10.3389/fbioe.2023.1165197.

Henry, G. B. L., A. Isenborghs, E. Walhain, T. Nicolay, B. A. Stenuit, and P. A. Gerin. 2024. "Enhancing the Fermentability of Brewer's Spent Grains to Short- and Medium-Chain Carboxylates Through Dilute Alkaline Pretreatment." *Biomass Conversion and Biorefinery* 15: 6435–6448. https://doi.org/10.1007/s13399-024-05508-2.

Hermann, M., A. Teleki, S. Weitz, et al. 2020. "Electron Availability in CO_2, CO and H_2 Mixtures Constrains Flux Distribution, Energy Management and Product Formation in *Clostridium ljungdahlii*." *Microbial Biotechnology* 13: 1831–1846. https://doi.org/10.1111/1751-7915.13625.

Hill, J. D., and E. T. Papoutsakis. 2025. "Understanding and Harnessing the Complexity of Interspecies Interactions in Acetogenic Mixotrophic Co-Cultures." *Current Opinion in Biotechnology* 93: 103311. https://doi.org/10.1016/j.copbio.2025.103311.

Hitch, T. C. A., K. Bisdorf, A. Afrizal, et al. 2022. "A Taxonomic Note on the Genus *Prevotella*: Description of Four Novel Genera and Emended Description of the Genera *Hallella* and *Xylanibacter*." *Systematic and Applied Microbiology* 45: 126354. https://doi.org/10.1016/j.syapm.2022.126354.

Holtzapple, M. T., H. Wu, P. J. Weimer, et al. 2021. "Microbial Communities for Valorizing Biomass Using the Carboxylate Platform to Produce Volatile Fatty Acids: A Review." *Bioresource Technology* 344: 126253. https://doi.org/10.1016/j.biortech.2021.126253.

Jarboe, L. R., L. A. Royce, and P. Liu. 2013. "Understanding Biocatalyst Inhibition by Carboxylic Acids." *Frontiers in Microbiology* 4: 272. https://doi.org/10.3389/fmicb.2013.00272.

Jourdin, L., T. Grieger, J. Monetti, et al. 2015. "High Acetic Acid Production Rate Obtained by Microbial Electrosynthesis From Carbon Dioxide." *Environmental Science & Technology* 49: 13566–13574. https://doi.org/10.1021/acs.est.5b03821.

Juvonen, R. 2015. "Strictly Anaerobic Beer-Spoilage Bacteria." In *Brewing Microbiology*, 195–218. Elsevier. https://doi.org/10.1016/B978-1-78242-331-7.00009-5.

Kang, S., H. Kim, B. S. Jeon, O. Choi, and B.-I. Sang. 2022. "Chain Elongation Process for Caproate Production Using Lactate as Electron Donor in *Megasphaera hexanoica*." *Bioresource Technology* 346: 126660. https://doi.org/10.1016/j.biortech.2021.126660.

Katsyv, A., A. Kumar, P. Saura, et al. 2023. "Molecular Basis of the Electron Bifurcation Mechanism in the [FeFe]-Hydrogenase Complex HydABC." *Journal of the American Chemical Society* 145: 5696–5709. https://doi.org/10.1021/jacs.2c11683.

Kim, B.-C. R., S. Kleinsteuber, and C. E. Lawson. 2025. "Carbon-Efficient Waste Upcycling: Combining Syngas Fermentation and Chain Elongation With Synthetic Consortia." *Current Opinion in Biotechnology* 94: 103321. https://doi.org/10.1016/j.copbio.2025.103321.

Kim, B.-C., B. Seung Jeon, S. Kim, H. Kim, Y. Um, and B.-I. Sang. 2015. "*Caproiciproducens galactitolivorans* Gen. Nov., sp. Nov., a Bacterium Capable of Producing Caproic Acid From Galactitol, Isolated From a Wastewater Treatment Plant." *International Journal of Systematic and*

Evolutionary Microbiology 65: 4902–4908. https://doi.org/10.1099/ijsem.0.000665.

Kim, H., S. Kang, and B.-I. Sang. 2022. "Metabolic Cascade of Complex Organic Wastes to Medium-Chain Carboxylic Acids: A Review on the State-of-the-Art Multi-Omics Analysis for Anaerobic Chain Elongation Pathways." *Bioresource Technology* 344: 126211. https://doi.org/10.1016/j.biortech.2021.126211.

Köpke, M., C. Held, S. Hujer, et al. 2010. "*Clostridium ljungdahlii* Represents a Microbial Production Platform Based on Syngas." *Proceedings. National Academy of Sciences. United States of America* 107: 13087–13092. https://doi.org/10.1073/pnas.1004716107.

Kotlar, C. E., M. Belagardi, and S. I. Roura. 2011. "Brewer's Spent Grain: Characterization and Standardization Procedure for the Enzymatic Hydrolysis by *Bacillus cereus* Strain." *Biotechnology and Applied Biochemistry* 58: 464–475. https://doi.org/10.1002/bab.62.

Kroneck, P. M. H., and M. E. S. Torres, eds. 2014. *The Metal-Driven Biogeochemistry of Gaseous Compounds in the Environment*. Springer Netherlands. https://doi.org/10.1007/978-94-017-9269-1.

Kucek, L. A., M. Nguyen, and L. T. Angenent. 2016. "Conversion of l-Lactate Into n-Caproate by a Continuously Fed Reactor Microbiome." *Water Research* 93: 163–171. https://doi.org/10.1016/j.watres.2016.02.018.

Łaba, W., M. Piegza, and J. Kawa-Rygielska. 2017. "Evaluation of Brewer's Spent Grain as a Substrate for Production of Hydrolytic Enzymes by Keratinolytic Bacteria." *Journal of Applied Chemistry and Biotechnology* 92: 1389–1396. https://doi.org/10.1002/jctb.5134.

Laura, M., and P. Jo. 2023. "No Acetogen Is Equal: Strongly Different H_2 Thresholds Reflect Diverse Bioenergetics in Acetogenic Bacteria." *Environmental Microbiology* 25: 2032–2040. https://doi.org/10.1111/1462-2920.16429.

Lee, N.-R., C. H. Lee, D.-Y. Lee, and J.-B. Park. 2020. "Genome-Scale Metabolic Network Reconstruction and In Silico Analysis of Hexanoic Acid Producing *Megasphaera elsdenii*." *Microorganisms* 8: 539. https://doi.org/10.3390/microorganisms8040539.

Liu, C., G. Luo, H. Liu, et al. 2020. "CO as Electron Donor for Efficient Medium Chain Carboxylate Production by Chain Elongation: Microbial and Thermodynamic Insights." *Chemical Engineering Journal* 390: 124577. https://doi.org/10.1016/j.cej.2020.124577.

Liu, X., and J. F. Salles. 2024. "Drivers and Consequences of Microbial Community Coalescence." *ISME Journal* 18: wrae179. https://doi.org/10.1093/ismejo/wrae179.

Lubitz, W., H. Ogata, O. Rüdiger, and E. Reijerse. 2014. "Hydrogenases." *Chemical Reviews* 114: 4081–4148. https://doi.org/10.1021/cr4005814.

Mariën, Q., A. Regueira, and R. Ganigué. 2023. "Steerable Isobutyric and Butyric Acid Production From CO_2 and H_2 by *Clostridium luticellarii*." *Microbial Biotechnology* 17: 14321. https://doi.org/10.1111/1751-7915.14321.

Mattarelli, P. 2018. "Chapter 2—Species in the Genus *Bifidobacterium*." In *The Bifidobacteria and Related Organisms: Biology, Taxonomy, Applications*, 9–48. Elsevier.

Miller, T. L. 2015. "Methanobrevibacter." In *Bergey's Manual of Systematics of Archaea and Bacteria*, edited by W. B. Whitman, 1st ed., 1–14. Wiley. https://doi.org/10.1002/9781118960608.gbm00496.

Mook, A., J. Herzog, P. Walther, P. Dürre, and F. R. Bengelsdorf. 2024. "Lactate-Mediated Mixotrophic Co-Cultivation of *Clostridium drakei* and Recombinant *Acetobacterium woodii* for Autotrophic Production of Volatile Fatty Acids." *Microbial Cell Factories* 23: 213. https://doi.org/10.1186/s12934-024-02481-3.

Nelson, R., D. Peterson, E. Karp, G. Beckham, and D. Salvachúa. 2017. "Mixed Carboxylic Acid Production by *Megasphaera elsdenii* From Glucose and Lignocellulosic Hydrolysate." *Fermentation* 3: 10. https://doi.org/10.3390/fermentation3010010.

Nzeteu, C. O., A. C. Trego, F. Abram, and V. O'Flaherty. 2018. "Reproducible, High-Yielding, Biological Caproate Production From Food Waste Using a Single-Phase Anaerobic Reactor System." *Biotechnology for Biofuels* 11: 4. https://doi.org/10.1186/s13068-018-1101-4.

Oelgeschläger, E., and M. Rother. 2008. "Carbon Monoxide-Dependent Energy Metabolism in Anaerobic *Bacteria* and *Archaea*." *Archives of Microbiology* 190: 257–269. https://doi.org/10.1007/s00203-008-0382-6.

Paradh, A. D., W. J. Mitchell, and A. E. Hill. 2011. "Occurrence of *Pectinatus* and *Megasphaera* in the Major UK Breweries." *Journal of the Institute of Brewing* 117: 498–506. https://doi.org/10.1002/j.2050-0416.2011.tb00497.x.

Perimenis, A., T. Nicolay, M. Leclercq, and P. A. Gerin. 2018. "Comparison of the Acidogenic and Methanogenic Potential of Agroindustrial Residues." *Waste Management* 72: 178–185. https://doi.org/10.1016/j.wasman.2017.11.033.

Poehlein, A., B. Zeldes, M. Flaiz, et al. 2025. "Advanced Aspects of Acetogens." *Bioresource Technology* 427: 131913. https://doi.org/10.1016/j.biortech.2024.131913.

Pot, B., G. E. Felis, K. D. Bruyne, et al. 2014. "The Genus *Lactobacillus*." In *Lactic Acid Bacteria*, edited by W. H. Holzapfel and B. J. B. Wood, 1st ed., 249–353. Wiley. https://doi.org/10.1002/9781118655252.ch19.

Prabhu, R., E. Altman, and M. A. Eiteman. 2012. "Lactate and Acrylate Metabolism by *Megasphaera elsdenii* Under Batch and Steady-State Conditions." *Applied and Environmental Microbiology* 78: 8564–8570. https://doi.org/10.1128/AEM.02443-12.

Schink, B. 1997. "Energetics of Syntrophic Cooperation in Methanogenic Degradation." *Microbiology and Molecular Biology Reviews* 61: 262–280. https://doi.org/10.1128/mmbr.61.2.262-280.1997.

Schwartz, E., J. Fritsch, and B. Friedrich. 2013. "H_2-Metabolizing Prokaryotes." In *The Prokaryotes*, edited by E. Rosenberg, E. F. DeLong, S. Lory, E. Stackebrandt, and F. Thompson, 119–199. Springer Berlin Heidelberg. https://doi.org/10.1007/978-3-642-30141-4_65.

Shah, H. N., M. A. Chattaway, L. Rajakurana, and S. E. Gharbia. 2015. "Prevotella." In *Bergey's Manual of Systematics of Archaea and Bacteria*, edited by W. B. Whitman, 1st ed., 1–25. Wiley. https://doi.org/10.1002/9781118960608.gbm00249.

Spirito, C. M., H. Richter, K. Rabaey, A. J. Stams, and L. T. Angenent. 2014. "Chain Elongation in Anaerobic Reactor Microbiomes to Recover Resources From Waste." *Current Opinion in Biotechnology* 27: 115–122. https://doi.org/10.1016/j.copbio.2014.01.003.

Spormann, A. M. 2023. *Principles of Microbial Metabolism and Metabolic Ecology*. Springer International Publishing. https://doi.org/10.1007/978-3-031-28218-8.

Standard Methods Committee of the American Public Health Association, American Water Works Association, and Water Environment Federation. 2023. "5220 Chemical oxygen demand (cod)." In *Standard Methods for the Examination of Water and Wastewater*. edited by W. C. Lipps, T. E. Baxter, and E. Braun-Howland. APHA Press. https://doi.org/10.2105/SMWW.2882.103.

Steffens, L., E. Pettinato, T. M. Steiner, et al. 2021. "High CO_2 Levels Drive the TCA Cycle Backwards Towards Autotrophy." *Nature* 592: 784–788. https://doi.org/10.1038/s41586-021-03456-9.

Suzuki, K. 2015. "Gram-Positive Spoilage Bacteria in Brewing." In *Brewing Microbiology*, 141–173. Elsevier. https://doi.org/10.1016/B978-1-78242-331-7.00007-1.

Tanner, R. S., L. M. Miller, and Y. Decheng. 1993. "*Clostridium ljungdahlii* sp. Nov., an Acetogenic Species in Clostridial rRNA Homology Group I." *International Journal of Systematic Bacteriology* 43: 232–263.

Tarasava, K., S. H. Lee, J. Chen, M. Köpke, M. C. Jewett, and R. Gonzalez. 2022. "Reverse β-Oxidation Pathways for Efficient Chemical

Production." *Journal of Industrial Microbiology & Biotechnology* 49: kuac003. https://doi.org/10.1093/jimb/kuac003.

Tremblay, J. 2019. *Amplicon Tagger Pipeline Databases*. Zenodo. https://doi.org/10.5281/zenodo.3560150.

Tremblay, J., K. Singh, A. Fern, et al. 2015. "Primer and Platform Effects on 16S rRNA Tag Sequencing." *Frontiers in Microbiology* 6: 771. https://doi.org/10.3389/fmicb.2015.00771.

Tremblay, J., and E. Yergeau. 2019. "Systematic Processing of Ribosomal RNA Gene Amplicon Sequencing Data." *GigaScience* 8: giz146. https://doi.org/10.1093/gigascience/giz146.

Ueki, A., H. Akasaka, A. Satoh, D. Suzuki, and K. Ueki. 2007. "*Prevotella paludivivens* Sp. Nov., a Novel Strictly Anaerobic, Gram-Negative, Hemicellulose-Decomposing Bacterium Isolated From Plant Residue and Rice Roots in Irrigated Rice-Field Soil." *International Journal of Systematic and Evolutionary Microbiology* 57: 1803–1809. https://doi.org/10.1099/ijs.0.64914-0.

Ueki, A., T. Shibuya, N. Kaku, and K. Ueki. 2015. "*Aminocella lysinolytica* Gen. Nov., sp. Nov., a l-Lysine-Degrading, Strictly Anaerobic Bacterium in the Class *Clostridia* Isolated From a Methanogenic Reactor of Cattle Farms." *Archives of Microbiology* 197: 97–104. https://doi.org/10.1007/s00203-014-1066-z.

Van Dijk, C., S. G. Mayhew, H. J. Grande, and C. Veeger. 1979. "Purification and Properties of Hydrogenase From *Megasphaera elsdenii*." *European Journal of Biochemistry* 102: 317–330. https://doi.org/10.1111/j.1432-1033.1979.tb04246.x.

Vögeli, B., L. Schulz, S. Garg, et al. 2022. "Cell-Free Prototyping Enables Implementation of Optimized Reverse β-Oxidation Pathways in Heterotrophic and Autotrophic Bacteria." *Nature Communications* 13: 3058. https://doi.org/10.1038/s41467-022-30571-6.

Wade, W. G. 2015. "Dialister." In *Bergey's Manual of Systematics of Archaea and Bacteria*, edited by W. B. Whitman, 1st ed., 1–5. Wiley. https://doi.org/10.1002/9781118960608.gbm00696.

Wallace, R. J., L. C. Chaudhary, E. Miyagawa, N. McKain, and N. D. Walker. 2004. "Metabolic Properties of *Eubacterium pyruvativorans*, a Ruminal 'Hyper-Ammonia-Producing' Anaerobe With Metabolic Properties Analogous to Those of *Clostridium kluyveri*." *Microbiology* 150: 2921–2930. https://doi.org/10.1099/mic.0.27190-0.

Wallace, R. J., N. McKain, N. R. McEwan, et al. 2003. "*Eubacterium pyruvativorans* Sp. Nov., a Novel Non-Saccharolytic Anaerobe From the Rumen That Ferments Pyruvate and Amino Acids, Forms Caproate and Utilizes Acetate and Propionate." *International Journal of Systematic and Evolutionary Microbiology* 53: 965–970. https://doi.org/10.1099/ijs.0.02110-0.

Wang, M., T. Yuan, J. Chen, et al. 2025. "A Species-Level Identification Pipeline for Human Gut Microbiota Based on the V3–V4 Regions of 16S rRNA." *Frontiers in Microbiology* 16: 1553124. https://doi.org/10.3389/fmicb.2025.1553124.

Wang, Y., W. Wei, X. Dai, L. Wu, X. Chen, and B.-J. Ni. 2023. "Different Electron Donors Drive the Variation in the Performance of Medium-Chain Fatty Acid Production From Waste-Activated Sludge." *ACS EST Engineering* 4: acsestengg.3c00423. https://doi.org/10.1021/acsestengg.3c00423.

Weimer, P. J., and G. N. Moen. 2013. "Quantitative Analysis of Growth and Volatile Fatty Acid Production by the Anaerobic Ruminal Bacterium *Megasphaera elsdenii T81*." *Applied Microbiology and Biotechnology* 97: 4075–4081. https://doi.org/10.1007/s00253-012-4645-4.

Wu, J., X. Zhang, P. Zhou, et al. 2017. "Improving Metabolic Efficiency of the Reverse Beta-Oxidation Cycle by Balancing Redox Cofactor Requirement." *Metabolic Engineering* 44: 313–324. https://doi.org/10.1016/j.ymben.2017.11.001.

Wu, S., N. Salmon, M. M.-J. Li, R. Bañares-Alcántara, and S. C. E. Tsang. 2022. "Energy Decarbonization via Green H_2 or NH_3?" *ACS Energy Letters* 7: 1021–1033. https://doi.org/10.1021/acsenergylett.1c02816.

Xu, J., J. Hao, J. J. L. Guzman, C. M. Spirito, L. A. Harroff, and L. T. Angenent. 2018. "Temperature-Phased Conversion of Acid Whey Waste Into Medium-Chain Carboxylic Acids via Lactic Acid: No External e-Donor." *Joule* 2: 280–295. https://doi.org/10.1016/j.joule.2017.11.008.

Zhao, S., R. Lau, Y. Zhong, and M.-H. Chen. 2024. "Lactate Cross-Feeding Between *Bifidobacterium* Species and *Megasphaera indica* Contributes to Butyrate Formation in the Human Colonic Environment." *Applied and Environmental Microbiology* 90: e01019. https://doi.org/10.1128/aem.01019-23.

Supporting Information

Additional supporting information can be found online in the Supporting Information section. **Data S1:** Supporting Information. **Data S2:** Supporting Information.